Published in final edited form as:
Neuroscience. 2012 June 28; 213: 161–178. doi:10.1016/j.neuroscience.2012.04.024.

Diverse populations of intrinsic cholinergic interneurons in the mouse olfactory bulb

Kurt Krosnowski[*], **Sarah Ashby**[*], **Aaron Sathyanesan**[*], **Wangmei Luo**, **Tatsuya Ogura**, and **Weihong Lin**
Department of Biological Sciences, University of Maryland, Baltimore County, Baltimore, MD 21250, USA

Abstract

Cholinergic activities affect olfactory bulb (OB) information processing and associated learning and memory. However, the presence of intrinsic cholinergic interneurons in the OB remains controversial. As a result, morphological and functional properties of these cells are largely undetermined. We characterized cholinergic interneurons using transgenic mice that selectively mark choline acetyltransferase (ChAT)-expressing cells and immunolabeling. We found a significant number of intrinsic cholinergic interneurons in the OB. These interneurons reside primarily in the glomerular layer (GL) and external plexiform layer (EPL) and exhibit diverse distribution patterns of nerve processes, indicating functional heterogeneity. Further, we found these neurons express ChAT and vesicular acetylcholine transporter (VAChT), but do not immunoreact to glutamatergic, GABAergic or dopaminergic markers and are distinct from calretinin-expressing interneurons. Interestingly, the cholinergic population partially overlaps with the calbindin D28K-expressing interneuron population, revealing the neurotransmitter identity of this sub-population. Additionally, we quantitatively determined the density of VAChT labeled cholinergic nerve fibers in various layers of the OB, as well as the intensity of VAChT immunoreactivity within the GL, suggesting primary sites of cholinergic actions. Taken together, our results provide clear evidence showing the presence of a significant number of cholinergic interneurons and that these morphologically and distributionally diverse interneurons make up complex local cholinergic networks in the OB. Thus, our results suggest that olfactory information processing is modulated by dual cholinergic systems of local interneuron networks and centrifugal projections.

The OB is the first central relay station in the vertebrate olfactory system (Mori et al., 1999, Shepherd et al., 2004). It receives rich afferent sensory information encoding odor molecule structure and concentration as well as spatiotemporal aspects of odor stimulation (Buck, 1996, Wachowiak and Cohen, 2001, Spors et al., 2006, Carey et al., 2009). This sensory information is processed and refined substantially by a diverse array of local interneurons that differ in spatial distribution, neurochemical expression and synaptic connections (Ojima et al., 1988, Hayar et al., 2004, Shipley et al., 2004, Wachowiak and Shipley, 2006, Parrish-Aungst et al., 2007, Cave and Baker, 2009, Shao et al., 2009, Kiyokage et al., 2010, Kosaka

Corresponding author: Weihong Lin, PhD Department of Biological Sciences, University of Maryland, Baltimore County, Baltimore, MD 21250, USA Phone: 410-455-8674 Fax: 410-455-3875 Weihong@umbc.edu.
[*]These three authors contribute equally.

and Kosaka, 2011, Sassoe-Pognetto, 2011). While GABAergic, dopaminergic and glutamatergic interneurons in the OB are well established, the existence of cholinergic interneurons in the OB is controversial. A few studies show a low number of bulbar ChAT-expressing cells in rats (Ojima et al., 1988, Phelps et al., 1992), but most studies failed to label cholinergic cell bodies in the OB using either immunolabeling or in situ mRNA hybridization in rats (Godfrey et al., 1980, Le Jeune and Jourdan, 1991, Butcher et al., 1992, Ichikawa et al., 1997) and hedgehog (Crespo et al., 1999). In addition, many studies showed various types of bulbar neurons, including output and local interneurons that are acetylcholinesterase (AChE)-positive in the OB. However, the results are inconclusive for the presence of cholinergic interneurons because AChE is present on both cholinergic and cholinoceptive neurons (Nickell and Shipley, 1988, Le Jeune and Jourdan, 1994, Kasa et al., 1996). Without consistent results of ChAT-ir in the OB, these early studies concluded that AChE-positive neurons are cholinoceptive and that cholinergic interneurons either do not exist or are insignificant because of low cell counts. This is in contrast to the rest of the central nervous system where there are a variety of cholinergic interneurons (Woolf, 1991, Krnjevic, 1993).

In the OB, cholinergic activities modulate glomerular microcircuits, the dendrodendritic reciprocal synapses between granule cells (GC) and mitral/tufted cells, and excitability of GC (Elaagouby et al., 1991, Nickell and Shipley, 1993, Castillo et al., 1999, Pressler et al., 2007, Ghatpande and Gelperin, 2009). These modulatory activities are important for odor discrimination, odor-guided behaviors and perceptual learning (Ravel et al., 1994, Doty et al., 1999, Fletcher and Chen, 2010). The OB receives extensive centrifugal cholinergic projections primarily from the horizontal limb of the diagonal band of Broca (HLDB) (Macrides et al., 1981, Carson, 1984, Zaborszky et al., 1986, El-Etri et al., 1999, Matsutani and Yamamoto, 2008). Due to the lack of conclusive evidence of the existence of intrinsic cholinergic interneurons in the rodent OB, the cholinergic modulation mentioned above is generally thought to be mediated exclusively by centrifugal projections.

The evident importance and complexity of cholinergic modulation of OB functions call for more investigation on intrinsic cholinergic interneurons. However, visualizing cell bodies of small-size cholinergic interneurons in the brain is challenging because ChAT protein is primarily located in presynaptic terminals, and low levels of ChAT protein in cell bodies could lead to negative labeling results (Oda and Nakanishi, 2000). Recently, using a transgenic approach, Shang et al. (2007) identified a significant number of local cholinergic interneurons in the fly antennal lobe, a brain region that is equivalent to the OB in mammals. These cholinergic interneurons form excitatory local circuits that modulate the tuning property of output neurons. Further, synapse loss in these neurons during aging modifies fly smell perception (Acebes et al., 2011).

We sought to identify OB intrinsic cholinergic interneurons using transgenic marking and immunolabeling of cholinergic markers. Based on our previous studies (Ogura et al., 2007, Ogura et al., 2010, Ogura et al., 2011), we chose to use a transgenic mouse line in which the expression of enhanced green fluorescent protein eGFP) is driven by the endogenous ChAT transcriptional regulatory elements within a bacterial artificial chromosome (BAC) ($ChAT^{(BAC)-}$ eGFP (Tallini et al., 2006). In this mouse line, eGFP expression in cholinergic cells has been characterized previously on both neurons and non-neuronal cells, which provides excellent visualization of these cells (Tallini et al., 2006, Ogura et al., 2007, 2010, Krasteva et al., 2011, Ogura et al., 2011). Because our study focused on bulbar cholinergic interneurons, whose presence has been controversial, we first optimized our methods so that we could efficiently detect and visualize the cell bodies and fine processes of these neurons. We also conducted olfactory peduncle lesion to reduce cholinergic centrifugal projection to the OB to unmask intrinsic elements. We further characterized intrinsic cholinergic

interneurons using various antibodies known to label different populations of bulbar interneurons. Our data provide clear evidence for the presence of a significant number of intrinsic cholinergic interneurons in the mouse OB. In addition, our data provide a detailed view on their diverse morphological features, distribution patterns and expression of neurochemical markers. Our results strongly suggest that these local cholinergic neurons play an important role in cholinergic modulation of olfactory processing.

Experimental procedures

Animals

Experiments were performed on 2.5 to 6 month old C57BL/6 background transgenic mice of both genders. The original ChAT$^{(BAC)}$-eGFP breeding pairs were kindly provided by Dr. M. I. Kotlikoff from Cornell University (Tallini et al., 2006). The offspring were genotyped for the presence of GFP using polymerase chain reaction (PCR). The expression of GFP in cholinergic cells in ChAT$^{(BAC)}$-eGFP mice was characterized previously (Tallini et al., 2006, Ogura et al., 2007, Krasteva et al., 2011, Ogura et al., 2011). All animal care and procedures were approved by the Animal Care and Use Committee of University of Maryland, Baltimore County.

Immunohistochemistry

Tissue preparation—Adult ChAT$^{(BAC)}$-eGFP transgenic mice were deeply anesthetized with tribromoethanol (Avertin 250 μg/g body weight), perfused transcardially with 0.1M phosphate buffer (PB), followed by a phosphate buffered fixative containing 3% paraformaldehyde, 19 mM L-lysine monohydrochloride and 0.23% sodium m-periodate (Lin et al., 2008). This procedure and fixative was used for all immunohistochemical experiments except for GABA immunolabeling. The OBs were harvested along with the brain, post-fixed for 1.5 hours and transferred to 0.1M phosphate buffered saline (PBS) with 25% sucrose overnight. The brain was then split along the midline and the individual bulbs with half of the brain were embedded in optimal cutting temperature (OCT) compound (Sakura finetek USA Inc, Torrance CA). Free-floating sagittal sections (35 μm thick) were cut, unless otherwise noted, using a cryostat (Microm international, Walldorf, Germany). For immunolabeling with an anti-GABA antibody, mice were perfused using a phosphate buffered fixative containing 0.25% glutaraldehyde and 4% paraformaldehyde. The OB and brain tissues were post-fixed overnight in the same fixative with 25% sucrose and cut into 20 μm thick free-floating sections.

Immunohistochemistry—For our “standard” immunolabeling, sections containing OB were rinsed in 0.1M PBS 3×10 minutes followed by 1.5 hour incubation in PBS buffered blocking solution containing 2% normal donkey serum, 0.3% Triton X-100 and 1% bovine serum albumin. Sections were then immunoreacted for 48 to 72 hours at 4^{o}C with primary antibodies against each of the following proteins: GFP (1:3000; cat# ab13970, Abcam, Cambridge, MA), PGP 9.5 (ubiquitin carboxyl-terminal hydrolase; 1:500; cat# AB1761, Chemicon, Temecula, CA), ChAT (1:500; cat# AB144P, Millipore, Billerica, MA), VAChT (1:500; cat# V5387, Sigma, St Louis, MO), GABA (1:5000; code No: mAB 3D5, SWANT, Bellinzona, Switzerland), calbindin D-28k (1:2000; code No: 300, SWANT), calretinin (1:1000; code No: 7699/3H, SWANT), tyrosine hydroxylase (TH; 1:3000; cat# 657012, Calbiochem, San Diego, CA), olfactory marker protein (OMP; 1:1000; cat# O7889, Sigma), glutamate decarboxylase 65 and 67 (GAD65/67; 1:500; cat# AB1511, Millipore), glutamate receptor type 2 and 3 (Glu2/3; 1:200; Clone ID:EP929Y, Epitomice, Inc., Burlingame, CA) and vesicular glutamate transporter 2(VGluT2: 1:2000; cat# AB5907, Millipore). After incubation with primary antibodies, sections were washed and reacted with secondary antibodies conjugated with either Alexa 555 or 647 (1:400; Invitrogen, Eugene, OR) or

DyLight 488 donkey anti-Chicken secondary antibody (1:200; Jackson ImmunoResearch, West grove, PA) for 1 hour at room temperature. Sections were mounted on slides with Fluoromount-G containing DAPI, which stains nuclei (SouthernBiotech, Birmingham, AL). In control experiments, primary antibodies were omitted, which resulted in negative labeling.

We also optimized our protocol by including the following additional treatment to our standard method, which we refer to in the text as “improved” or “optimized” method. To enhance the ChAT-ir, we followed an optimized method, which had enabled us to successfully identify cholinergic microvillous cells in the olfactory epithelium (Ogura et al., 2011). In this method, antigen retrieval was performed in which OB sections were treated with 1M NaOH for 1 to 2 minutes, followed by three 30s rinses of 0.1M Na acetate and three10 minutes washes with 0.1M PBS before being transferred to the blocking solution. Additional treatments were also performed for immunolabeling of GABA in which sections were frozen and thawed three times by dipping in liquid nitrogen to increase permeability (Gracia-Llanes et al., 2003).

Image acquisition—Low magnification images were taken using an Olympus BX 41 epi-fluorescence compound microscope equipped with a Retiga 4000R camera (QImaging, British Columbia, Canada) and Image-Pro Plus 6.2 (Media cybernetics, Bethesda, MD). For images used for quantifying cholinergic nerve fibers, we used the same parameters for image capture, including exposure time and camera gain for the consistency of the analysis. The image resolution was 1.86 μm/ pixel with a 4x objective lens, which yields a threshold of 3.72 μm for distinguishing two adjacent fibers. High magnification images of immunolabeled sections were taken using an Olympus BX 61 epifluorescence microscope equipped with a spinning disc confocal unit and Slidebook 4.0 software (3i, Denver, CO).

Cell count and density estimation—Cholinergic (GFP-ir) and TH-expressing (TH+) or calbindin-expressing (CB+) interneurons were counted and used to determine the cell density of each cell type per layer and the estimated number of each cell type per OB. Cell counts were performed manually on randomly selected bulb areas covering 1/3 to 2/3 of every sixth OB section, cut sequentially. Epifluorescence images were taken in varying regions using a 10X lens. To determine cell density, the number of counted cells was divided by the total volume of each layer counted. The volume of each layer that was counted was determined by measuring the counted areas of each bulbar layer using the NIH imageJ program and multiplying the resulting area by the section thickness. To calculate the estimated cell number in a bulb, the cell density of each cell type in each bulb layer was then multiplied by the total bulb volume occupied by each layer. To estimate the total volume of each layer, we determined a standard bulb volume for each layer by measuring the area occupied by each layer from every 8th serial coronal section (18 μm thick), cut perpendicular to the lateral tract (Lin et al 2007) counterstained with DAPI, and multiplying this number by the section thickness. These section volumes were used to determine the total layer volumes per bulb using the Cavalieri method (Rosen and Harry, 1990). The volumes of each layer were averaged from three mice to generate a standard bulb volume.

To determine whether cholinergic interneurons are equally or unequally distributed between typical and atypical glomeruli, which receive heavy cholinergic innervation, GFP-ir interneurons surrounding individual atypical glomeruli were counted using every sixth sequential OB section (35 μm thick). The number of GFP-ir per typical glomerulus was calculated using the GFP-ir cell count obtained for the cell density estimation divided by the number of glomeruli in the counted areas.

Unilateral olfactory peduncle lesion

The surgical procedure was adapted from (Le Jeune and Jourdan, 1991). Adult mice were anesthetized and the skulls were exposed. An approximately 2.5 mm long incision, starting from the sagittal suture towards the lateral, was made on the skull 1 mm posterior to the coronal suture using a fine, hand-held sculpture drill. A thin plastic blade was inserted into the dorsal brain surface in parallel to the coronal suture and driven down to the bottom of the frontal brain at the level of the olfactory nucleus, just slightly off the medial region to avoid the major artery. The blade was then moved laterally to make a complete cut through the lateral brain region. After the surgery, the skin was sealed with LiquiVeT tissue adhesive (Oasis medical, Metta, Illinois). These mice were euthanized ten days after surgery for whole brain examination and immunohistochemical experiments.

Quantification of cholinergic nerve processes using line intensity profile analysis

We measured cholinergic nerve fiber density in the OB using our newly developed method (Sathyanesan et al., 2012) based on line intensity scan analysis using an image processing filter and peak detection algorithm. First, immunofluorescence images of VAChT immunoreactivity (VAChT-ir) were taken using a 4X lens from sequential OB sections (210 μm apart). The images were processed using a Hessian-based filter (Sato et al., 1998) in the NIH ImageJ software plugin, FeatureJ [Meijering E. (http://www.imagescience.org/meijering/software/featurej/)] to extract features of curvilinear objects (fibers). Using the segmented line tool of Image J, segmented lines were drawn through the glomerular layer (GL), external plexiform layer (EPL), internal plexiform layer (IPL) and granule cell layer (GCL) individually, parallel to the outer edge of each layer. Fluorescence intensity values along the line drawn on the image were extracted as a line intensity profile, *i.e.,* Line intensity scan. Background fluorescence intensity was set to the average intensity of a line intensity scan from the olfactory nerve layer (ONL), where there is no detectable VAChT-ir. Next, a peak-detection algorithm from the MATLAB Bioinformatics toolbox , “mspeaks,” was used to detect fibers represented as intensity peaks on the individual line scans, only if the peaks were higher than the mean background intensity (from the ONL) of the unfiltered image. The total number of peaks was then divided by the length of each individually drawn segmented line to yield the average number of peaks per 100 μm line. For fiber density analysis, we performed an additional set of line scans perpendicular to the curvature of the parallel line scan. This was done to account for the fibers running parallel to the layer edges. A total of 5 scans were performed at different points along the EPL (posterodorsal, mediodorsal, anterodorsal, anteroventral and posteroventral) for sections in which the different layers were clearly distinguishable. The number of peaks obtained through the parallel scans and the mean number of peaks obtained through the perpendicular scans were multiplied to yield total number of peaks per unit area. This was done based on the assumption that fiber density along the two sets of scans were: 1) non-repetitive and 2) uniformly distributed (as we did not observe any regions with statistically higher intensity within a layer). To account for the thickness of sections, we divided the resulting number by the thickness of the tissue section (35μm), resulting in a fiber-count per μm^3. Final units are however in terms of number of fibers/$(100\ \mu m)^3$, which can also be seen as the number of fibers in a cubic volume of tissue with side 100 μm. Mean number of fibers/$(100\ \mu m)^3$ was calculated (n=3 bulbs). For comparison of nerve fiber density in olfactory bulbs from mice with unilateral olfactory peduncle lesion, sections from both olfactory bulbs of individual mice were immunolabeled side by side, imaged and processed under the same conditions.

Data analyses

Student's t-tests (unpaired, one-way) were used to compare intensity of VAChT immunolabeled nerve fibers in glomerular neuropiles and periglomerular (PG) regions, as

well as fiber scan densities of individual layers between right and left bulbs from mice with unilateral olfactory peduncle lesion. Statistical analyses were performed using Origin 6.0 graphing software and $p < 0.05$ was considered statistically different.

Results

GFP expression and immunoreactivity of cholinergic markers in brain cholinergic interneurons

For quantitative and morphological characterization of cholinergic interneurons in the mouse OB, it is important that our methods are optimized so that local cholinergic interneurons and their fine processes in the OB can be efficiently visualized. We chose sagittal brain sections for this purpose because there are a variety of well characterized cholinergic neurons in various brain regions (Woolf, 1991) and we could monitor both brain and bulbar neurons in the same sections. In addition, a close examination of GFP signal and immunoreactivity for ChAT and VAChT in the same neurons also allowed us to further evaluate the ChAT$^{(BAC)}$-eGFP mice. Further, the difference between results obtained from the standard and improved methods might provide an explanation for the previous inconsistent findings about bulbar cholinergic interneurons (Phelps et al., 1992, Ichikawa et al., 1997). A collection of representative GFP-expressing and ChAT- or VAChT-immunolabeled brain cholinergic neurons from sections of ChAT$^{(BAC)}$-eGFP mice is shown in Fig. 1. Consistent with the results from Tallini et al (2006), we found GFP fluorescence signal in cell bodies and nerve processes of numerous neurons in various brain regions. The intensity levels of GFP fluorescence varied considerably among these cell bodies and processes. Whereas cell bodies of large-diameter (usually larger than 15 μm), multi-polar ChAT immunoreactive neurons in the ventral brain and striatum exhibited very bright GFP fluorescence, the GFP signal in fine nerve processes was modest or weak (pointed by arrows in Fig. 1A). We amplified the GFP signal using an anti-GFP antibody in immunolabeling experiments, which resulted in better visualization of the distal fine processes, as well as small-diameter neurons throughout brain sections (Fig. 1B). Thus, for all other GFP-related results presented in this paper, we used the anti-GFP antibody, along with other antibodies of interest. The intensity of ChAT-ir also varied among neuronal cell bodies and processes. Using our standard labeling method, we found that the ChAT antibody strongly immunolabeled large-diameter, multi-polar cholinergic neurons and their proximal processes, but failed to label many fine nerve processes that are positive for GFP (pointed by arrows in Fig. 1A). From our previous studies, we knew the intensity of ChAT-ir depends heavily on the labeling method (Ogura et al., 2007, 2011). Therefore, we tried various approaches and found that adding the treatment of antigen retrieval to our standard method enhanced the ChAT-ir in all cellular regions, including fine distal processes (Fig. 1B). Using this optimized method, we were able to observe ChAT-ir in local GFP-ir interneurons in the hippocampus and cortex (Fig. 1C and D, respectively, inset: a ChAT immunoreactive cell). In the cortex and hippocampus, almost all the GFP-ir cells examined were positive for ChAT-ir, while approximately 13% ChAT-immunoreactive cortical neurons did not show detectable GFP-ir (pointed by arrows in Fig. 1D; calculated from a total 136 cells from random images from 3 mice). The ChAT–ir in hippocampal and cortical interneurons were relatively weak as compared to those large-diameter cholinergic neurons shown in Fig. 1A and B. We closely monitored these small-diameter (usually less than 13μm) cholinergic neurons for our method optimization. This is because, similar to the bulbar cholinergic interneurons, these interneurons are not easily labeled by anti-ChAT antibodies as compared to large-diameter cholinergic neurons and some studies failed to show their presence (for review, see Oda and Nakanishi, 2000). These results provide direct co-localization of GFP signal and ChAT-ir in cell bodies and fine processes of these brain cholinergic interneurons, as well as a view of amazingly complex cholinergic networks in these regions. Also our data

show that both GFP expression and the intensity of ChAT-ir could vary among cholinergic cells, which likely reflects the different levels of ChAT proteins expressed. Thus, an anti-ChAT antibody that can successfully label the large-diameter cholinergic neurons, may not produce detectable labeling in the small-diameter neurons if the methods are not sufficiently sensitive.

We next examined the immunolabeling for the other cholinergic marker VAChT, which is responsible for transporting cytosolic ACh into synaptic vesicles (Arvidsson et al., 1997). As shown in Fig. 1E, the anti-VAChT antibody intensely labeled numerous fine nerve processes that are positive for GFP-ir. The VAChT-ir was also strong in the cell bodies and proximal region of these large-diameter neurons (Fig. 1 E"; GFP-ir of these cells in E'), although in the distal regions of these processes, the labeling was only modest or sometimes undetectable (Fig. 1E and E"). Fig. 1F shows a representative image of large-diameter cholinergic interneurons in the striatum. The immunoreactivity of ChAT, VAChT and GFP are co-localized in these neurons. In the hippocampus, strong VAChT-ir was seen in numerous GFP-ir processes (Fig. 1G), which is similar to the ChAT-ir shown in Fig. 1C. But in the cell bodies of the GFP-ir small-diameter local interneurons, the VAChT-ir was generally weak or undetectable by our current methods (Fig. 1G), which is in contrast to the bright VAChT-ir in the cell bodies of large-diameter neurons in Fig. 1E and E". A magnified image of VAChT-ir in bouton-like or varicose structures of GFP-ir nerve fibers is shown in Fig. 1G, inset. These results are consistent with the notion that ChAT and VAChT proteins are located primarily at presynaptic terminals where ACh synthesis, storage and release take place (Weihe et al., 1996). Thus, in our study, the combination of GFP-ir, ChAT-ir and VAChT-ir provided a better visualization of cholinergic cell bodies and fine processes as well as regions where cholinergic activities likely take place.

Cholinergic nerve fibers in the OB of ChAT$^{(BAC)}$-eGFP mice visualized by GFP, ChAT and VAChT immunoreactivity

In sagittal OB sections of ChAT$^{(BAC)}$-eGFP mice, we observed numerous GFP-ir nerve fibers as well as local interneuron cell bodies, which we will describe in detail in later paragraphs. In the main olfactory bulb (MOB), the GFP-ir nerve fibers were abundantly present in the GL, EPL, IPL and GCL (Fig. 2A). Occasionally, few GFP-ir nerve processes were found in the ONL (data not shown). The origin of these GFP-ir nerve fibers in the ONL is not known. But they are not axons from olfactory sensory neurons (OSNs) since we did not observe any OSNs expressing ChAT (Ogura et al., 2011). We immunolabeled OB sections with the anti-ChAT antibody, which labeled the GFP-ir nerve fibers confirming that they are cholinergic (Fig. 2A; A': ChAT-ir alone). In the EPL, GFP-ir fibers run either in parallel to the MCL, especially in the deep region of the EPL, or towards the GL. Further, the GFP-ir fibers were also immunoreactive to the antibody against VAChT. Fig. 2B shows co-localization of the immunoreactivity of GFP, ChAT and VAChT, which is especially obvious in some glomeruli that receive dense cholinergic innervation in the GL of the caudal bulb (pointed by arrows in Fig. 2B). These glomeruli resemble the appearance of atypical glomeruli (Le Jeune and Jourdan, 1991, Shinoda et al., 1993). Further, when closely examined, we found the GFP-ir fibers were not restricted in their own layers. As shown in Fig. 2C and D, respectively, some GFP-ir fibers exited the IPL and passed the MCL to enter the EPL and many GFP-ir fibers were found traveling between the EPL and GL. In sections cut through the GL and immunolabeled with antibodies against GFP, VAChT and ChAT, we found GFP-ir fibers present in periglomerular (PG) areas as well as within glomerular neuropiles (Fig. 2E). The intensity of VAChT-ir was stronger in the neuropiles, as compared to the surrounding PG areas, suggesting that neuropiles are primary sites for ACh release within the GL. To further characterize cholinergic fibers within individual glomeruli, we labeled axon terminals of OSNs in OB sections with antibodies against either olfactory

marker protein (OMP) (Fig. 2F) or vesicular glutamate transporter 2 (VGluT2) (Fig. 2G). It is known that a glomerulus can be compartmentalized into olfactory nerve (ON) zones and non-ON zones (Kosaka and Kosaka, 2005). Both anti-OMP and VGluT2 labeled ON zones. We found that GFP-ir fibers were more apparent in the non-ON zones lacking OMP and VGluT2 immunoreactivity. Taken together, our combined approaches of transgenic marking and ChAT and VAChT immunolabeling provided a detailed view of the extensiveness of cholinergic fiber networks in the OB and differences within individual layers.

Quantitative analysis of cholinergic fiber density

We next quantitatively determined the density of cholinergic fibers in individual bulbar layers of the entire OB section using our newly developed method for direct fiber counting (Sathyanesan et al., 2012). This method, which primarily makes use of Hessian-based feature extraction (Sato et al., 1998) and line intensity profiling, allows us to sample nerve fiber intensity across large brain regions, ensuring thorough sampling (Sathyanesan et al., 2012). For this measurement, we did not rely on GFP signal because there were many GFP-expressing interneuron cell bodies in the bulb. Instead, we conducted our density measurements on VAChT immunolabeled cholinergic fibers because the antibody strongly labeled GFP-ir fibers and the labeling in cell bodies was generally weak or absent except in focal spots where nerve processes protrude. Fig. 3A shows VAChT-ir in a representative sagittal OB section where the actual line intensity scans were conducted. An enlarged image of VAChT-ir, with dashed lines drawn in each bulbar layer representing individual parallel line intensity scans, is shown in Fig. 3B (The perpendicular scan lines are not shown). Both these images were processed using Hessian-based feature extraction in NIH ImageJ, which enhanced the curvilinear features, *i.e.* nerve fibers in the images (Sathyanesan et al., 2012). A raw image from an EPL region before Hessian feature extraction is provided in Fig. 3A, inset for comparison. Fig. 3C shows sample line intensity profiles of VAChT-immunolabeled nerve fibers, which correspond to the intensity along the dashed lines in Fig. 3B. Each intensity peak in the profiles represents a hit of a single VAChT-labeled nerve fiber. The number of fibers was determined by counting all the peaks that show intensity values higher than the extracted background intensity threshold from a scan in the ONL where there is no VAChT label. We verified the method with randomized manual counting, which yielded very similar results. Because of the dense fiber clusters in a few atypical glomeruli in the caudal OB, we avoided these glomeruli when scanning the GL. For the actual scans that were conducted in the entire bulb sections, the average lengths of the parallel scans per bulb were 26.3 mm (GL), 23.9 mm (EPL), 20.5 mm (IPL) and 18.3 mm (GCL) (n = 3 bulbs from three mice). The fiber densities of these layers are listed in Table 1. Fig. 3D shows the histogram of intensity distribution for VAChT-immunolabeled nerve fibers in various layers from parallel scans conducted on sagittal OB sections. More VAChT-labeled nerve fibers in the IPL and GL show relatively higher intensity values, whereas a higher fraction (~80%) of the nerve fibers counted in EPL show lower intensity values, suggesting layer differences in cholinergic activities. Further, we calculated fiber density per volume based on the parallel scans and 5 additional line scans perpendicular to the parallel scans conducted in each layer, as well as the section thickness. The average density values of VAChT-immunolabeled nerve fibers for individual layers are plotted in Fig. 3E. The density values of cholinergic nerve fibers in the IPL and GL were higher than those in the EPL and GCL, further suggesting the IPL and GL are major sites for cholinergic modulation. Our results are comparable to published cholinergic fiber densities in the brain (Mechawar and Descarries, 2001). These data provide the first thorough and quantitative measurement of the elaborate cholinergic fiber network in the OB.

Because the VAChT-ir in the GL was apparently stronger within the glomerular neuropiles than in the surrounding PG regions (Fig. 3F, see also Fig. 2E), we conducted intensity

measurements in randomly selected glomeruli and their PG regions to quantitatively evaluate the cholinergic action sites in the GL. The average intensity values of VAChT-ir in neuropiles and PG regions are plotted in Fig. 3G, showing that within the GL, the VAChT-ir intensity is significantly higher in neuropiles than in surrounding PG regions (20 neuropiles and 10 PG regions measured). Because the higher area intensity in the neuropiles could potentially result from more VAChT-labeled nerve fibers, we conducted line intensity scans through randomly selected glomeruli and their PG regions (10 glomeruli, 6 PG regions). The result shows that the average intensity value of VAChT-labeled nerve fibers was significantly higher in neuropiles than in PG regions (Student's T-test, $p < 0.05$, Fig. 3H). These results strongly suggest that glomerular neuropiles are the primary sites in the GL for cholinergic actions.

Intrinsic cholinergic interneurons in the olfactory bulb

Noticeably, from images in Fig. 2, there are many GFP-ir interneurons in various regions of the MOB. The GFP-ir in the cell bodies varied significantly, from very bright to faint. The largest group of these neurons was found in the GL surrounding individual glomeruli. The second largest group was found in the deep region of the EPL, close to the MCL. The cell bodies of these neurons were either scattered or grouped in small patches. In addition, there were some GFP-ir interneurons scattered in other regions of the EPL, MCL and IPL, and few in the GCL. We counted the number of GFP-ir positive cells in various layers and determined the cell density. Cell counts from the EPL, MCL and IPL were pooled because some of these GFP-ir cells were located in the border regions between these layers. Also, we calculated the total volume of the GL, EPL/MCL/IPL and GCL per bulb to estimate the total cell counts and density for these layers and a whole bulb. Table 2 lists the averaged GFP-ir cell count, cell densities and the extrapolated total numbers of these GFP-ir interneurons in various layers per OB. Based on the calculated volumes, there are an average of 30,440 +/- 3775 and 37,108 +/- 3706 cholinergic interneurons in the GL and whole bulb respectively (n= 8 bulbs from 8 mice). These quantitative results clearly show a significant number of cholinergic interneurons in the MOB.

In addition, we also conducted a cell count to determine whether there is differential distribution of the cholinergic PG cells between typical and atypical glomeruli since Crespo et al. (1996, 1997) reported that some juxtaglomerular (JG) interneurons are distributed statistically higher surrounding typical glomeruli than atypical glomeruli. From a total of 124 atypical glomeruli examined (n=4 mice), the average GFP-ir interneurons per atypical glomerulus was 2.3 and GFP-ir interneurons per typical glomerulus was 6.3 averaging from 854 glomeruli per 35 μm thick OB sections (n=4 mice). Thus, in general there are about 2.7 times more GFP-ir interneurons surrounding typical glomeruli.

Morphological features of the intrinsic cholinergic interneurons

The above results reveal the co-existence of both intrinsic and centrifugal cholinergic systems. However, the extensive centrifugal nerve processes make detailed characterization of the intrinsic nerve processes and their distribution patterns difficult, especially in the GL. Thus, we conducted olfactory peduncle lesioning, which is known to reduce centrifugal projections to the OB (Wenk et al., 1977, Zheng et al., 1987). In most of our mice, the surgical disruption was slightly incomplete to avoid damage of the major blood vessel in the medial-ventral floor of the brain. The density values of VAChT-ir fibers measured in the MOB, both ipsilateral and contralateral to the surgery site, are listed in Table 1 (n=3 mice). Fig. 4A shows a representative image of GFP-ir and ChAT-ir from an OB section ipsilateral to the lesion. In comparison to the contralateral OB, the reduction of the fiber density in all layers of the ipsilateral OB, except the ONL, was significant. Also in these ipsilateral OBs, the dense cholinergic innervation in the atypical glomeruli was lost (Fig. 4B: contralateral,

Fig. 4C: ipsilateral). Interestingly, when compared to the GL of control OBs (Fig. 4D), the nerve fibers in PG regions were greatly diminished in OB sections ipsilateral to the surgery, whereas within the glomeruli, considerable numbers of GFP-ir nerve processes remained and were from local interneurons (Fig. 4E).

Importantly, the olfactory peduncle lesion allowed us to clearly observe the morphology of intrinsic GFP-ir interneurons in various OB layers. We found that in the GL, most of the GFP-ir interneurons are PG cells with apical processes ramifying in single glomeruli (Fig. 4E and Fig. 5A, higher magnification representative images in Fig. 5B and C). Interestingly, a single branch from a GFP-ir PG cell could arborize extensively to form a small plexus (pointed by an arrow in Fig. 5C) in a region corresponding to the non-ON zone within a glomerulus (see also Fig. 2F and G). A few GFP-ir interneurons in the GL apparently sent their processes to more than one glomerulus (Fig. 5A pointed by an arrow and Fig. 5D, high magnification). This type of interneuron can be considered juxtaglomerular (JG) cells, since their processes are not limited to a single glomerulus (Kiyokage et al., 2010, Kosaka and Kosaka, 2011). In the EPL, MCL and IPL, the GFP-ir neurons can be sub-divided into three groups based on the morphology and distribution of their nerve processes. The first group of GFP-ir neurons resided primarily in the deep EPL with some in the MCL. These cells emanated two to three processes from their cell bodies, and their primary processes ran across the EPL and towards the GL, some of which apparently innervated glomeruli (Fig. 5E and F). The second group of GFP-ir neurons also resided in the deep EPL and in the MCL. Unlike the first group, they were bipolar, with two processes protruding from opposite ends of the cell bodies. Their primary processes were usually long and thick and ran in parallel to the MCL. Some of these processes could be traced as long as half the bulb in sagittal sections (Fig. 5 G and H). This subtype of cholinergic interneurons had been briefly described by Phelps et al (1992). In general, the primary nerve processes of these two groups of GFP-ir interneurons were relatively thick and easy to distinguish. In contrast, the third group of GFP-ir neurons usually had many intricate local processes. Most of these cells resided in regions of the deep EPL, MCL and IPL. A few of them resided in the mid EPL. Representative images of these neurons from the deep and middle regions of the EPL are shown in Fig. 5I, J and K, respectively. Fig. 5L and M show two GFP-ir interneurons in the IPL with distinct morphology. Few GFP-ir cells also were seen in the GCL. Fig. 5N shows such a neuron with many synaptic spine-like structures in its nerve processes, which resembles a ChAT-ir interneuron described in Phelps et al (1992). These results provide a detailed view on the diverse morphological features of cholinergic interneurons within the MOB, suggesting distinct functions of these interneurons.

Immunoreactivity of ChAT and VAChT in cell bodies of GFP-ir interneurons

Our study using transgenic mice provides strong evidence of intrinsic cholinergic interneurons in the MOB. To further demonstrate GFP-ir interneurons were cholinergic, we immunolabeled OB sections with antibodies against either ChAT or VAChT. Fig. 6A and B show typical images of GFP and ChAT immunolabeling in the GL, respectively (overlaid image in Fig. 6C; higher magnification representative images in Fig. 6D and E). ChAT-ir was present in numerous nerve fibers as well as GFP-ir cell bodies in the MOB. The intensity of ChAT-ir in the cell bodies was either similar to the intensity of the surrounding nerve fibers or weaker. We purposely present the image of Fig. 6B, in which representative ChAT-ir cell bodies are pointed by red arrows, to demonstrate that had we not had GFP-ir to mark these cell bodies, it would have been difficult to find them in the presence of extensive ChAT-immunoreactive nerve fibers. Therefore, for clarity, we performed VAChT immunolabeling on OB sections ipsilateral to the olfactory peduncle lesion site. Fig. 6F shows a representative image of VAChT-ir in two glomeruli. Most of the VAChT-ir was observed in the processes within the glomeruli, and there were little or no nerve fibers

labeled with VAChT surrounding the glomeruli. Individual GFP-ir cell bodies were also positively labeled with VAChT (Fig. 6F and G). Interestingly, the VAChT-ir was not uniformly distributed in these cell bodies. Instead, the VAChT-ir concentrated in particular regions, where the major processes emanate (pointed by arrows in Fig. 6F and G). A similar pattern of VAChT-ir was observed in GFP-ir cholinergic interneuron cell bodies and nerve processes in other bulbar layers. Fig. 6H shows a representative image of VAChT-immunoreactive cells in the EPL (overlaid image in Fig. 6I; Arrows point strong VAChT-ir in the particular regions in the cell bodies). Note that the distal ends of the processes in these cells were also strongly positive for VAChT-ir. The positive immunoreactivity for both cholinergic markers, ChAT and VAChT, in GFP-ir cell bodies provides additional strong evidence for the presence of intrinsic cholinergic interneurons in the MOB.

The GFP-ir neurons in the MCL are not mitral cells

The MCL contains both output neurons and local interneurons (Frazier and Brunjes, 1988, Parrish-Aungst et al., 2007). Because we found many GFP-ir cells in the deep region of the EPL as well as in the MCL and IPL, we investigated whether these GFP-ir cells are distinct from the glutamatergic mitral/tufted cells since previous studies show some mitral cells express AChE (Nickell and Shipley, 1988). We immunolabeled mitral/tufted cells using antibodies against a neuronal marker, PGP 9.5, which provides an outstanding morphological view of these neurons (Nakajima et al., 1998), and glutamate receptor subunits 2/3 (GluR2/3), a marker for glutamatergic neurons. In sections labeled with the PGP 9.5 antibody, we found that GFP-ir interneurons were labeled, indicating they were neurons (Fig. 7A; A': GFP-ir alone). Fig. 7B showed the MCL region of Fig. 7A (the lower middle region; 7B': PGP9.5-ir alone). Fig. 7C and C' show another view of the immunolabeling in the deep EPL and the MCL. These images clearly show that GFP-ir cells had smaller cell bodies and relatively thin nerve processes (arrows in Fig. 7B' and C' point representative GFP-ir cell bodies). In contrast, mitral/tufted cells exhibited larger cell bodies and distinct primary and secondary dendrites. In sections labeled with the GluR2/3 antibody, we found none of the GFP-ir cells in the MOB was immunoreactive for GluR2/3 (Fig. 7D; D': GluR2/3-ir alone). Further, we measured the cell body diameters of GFP-ir cells and mitral/tufted cells. The averaged diameter of GFP-ir cell bodies was about 50% smaller than that of mitral/tufted cells (Fig. 7E). Thus, the GFP-ir cells in the MCL of the MOB clearly were neither mitral/tufted cells nor glutamatergic.

Cholinergic interneurons in the GL and EPL do not immunoreact to dopaminergic, GABAergic or glutamatergic markers

Previously described interneurons in the OB express various neurotransmitters, such as dopamine, GABA and glutamate (Baker et al., 1983, Shipley et al., 2004, Bovetti et al., 2007, Kosaka and Kosaka, 2011). The dopaminergic (DA+) interneurons in the GL are GABAergic (Parrish-Aungst et al., 2007). We used antibodies to mark these cell types to determine whether the cholinergic interneurons form a distinct population. In OB sections labeled with the antibody against TH, a rate-limiting enzyme for the biosynthesis of dopamine (Cave and Baker, 2009), we found that TH immunoreactivity (TH-ir) was present in a subset of interneurons, which resided mostly in the GL and few in the EPL. Fig. 8A shows TH-ir, and GFP-ir within a glomerulus and surrounding PG interneurons with DAPI staining outlining the glomerulus (A': TH-ir with DAPI; A": GFP-ir; Fig. 8B: higher magnification). None of the GFP-ir cells were labeled with the TH antibody. We conducted cell counts for GFP-ir and TH+ cells in various layers. The averaged ratio of GFP-ir to TH+ cells in the GL and EPL/MCL/IPL are 0.64 and 3.83, respectively. The overall ratio calculated from the total counted cells is about 0.76 (3 bulbs from three mice, averaging 2997 +/-193 cells counted per bulb; Table 3).

To label the GABAergic interneurons, we used antibodies against either glutamic acid decarboxylase isotypes 65 and 67 (GAD65/67) or GABA. We found that the anti-GAD 65/67 antibody did not label any GFP-ir interneurons either in the EPL (C: overlaid image of GAD 65/67-ir, GFP-ir and DAPI; C': GAD 65/67-ir with DAPI showing the layer organization; C": GFP-ir) or in the GL (D: overlaid image of GAD 65/67-ir, GFP-ir and DAPI; D': GAD 65/67-ir; D": GFP-ir with DAPI outlining individual glomeruli). A similar result was obtained with the anti-GABA antibody (data not shown). Further, we examined the GluR2/3-expressing interneurons in the GL, since some JG cells, such as short axon cells and external tufted cells, are excitatory and glutamatergic (Aungst et al., 2003). We found the anti-GluR2/3 antibody labeled a subset of JG cells. None of them were GFP-ir cells (Fig. 8E; overlaid image of GluR 2/3-ir, GFP-ir and DAPI; E': GluR 2/3-ir with DAPI; E": GFP-ir; Fig. 8F: higher magnification). Additionally, we examined GFP-ir cells in other layers and none of them reacted to these antibodies (Data not shown). Thus, our results demonstrate that cholinergic interneurons in the MOB are not dopaminergic, GABAergic or glutamatergic.

A majority of cholinergic interneurons express a calcium-binding protein calbidin D28K

MOB interneurons are known to express various calcium binding proteins, including parvalbumin, calretinin (CR), calbindin D28K (CB) and neurocalcin and have been classified into distinct chemotypes based on their expression (Parrish-Aungst et al., 2007, Kosaka and Kosaka, 2008, 2010, 2011). It has been estimated that about 13% of the total GL neurons are calbindin positive (CB+) of which approximately 60% are GABAergic based on GAD 67 expression (Parrish-Aungst et al., 2007). The neurotransmitter identity in the remaining CB+ interneurons is not determined. We investigated whether the cholinergic cells co-express CB or CR. In sections labeled with antibodies against GFP, CR and CB, we found CB and CR were expressed in two non-overlapping populations of interneurons in various layers of the MOB (Fig. 9A; Enlarged images showing single populations of GFP-ir, CB-ir and CR-ir from the GL region marked in panel A are shown in Fig. 9B, C and D). We examined on average 3559 +/- 509 GFP-ir cells per MOB from three adult ChAT$^{(BAC)}$-eGFP mice and found none were calretinin positive. Interestingly, we found that GFP-ir neurons and CB+ neurons overlapped (Fig. 9E; and Fig. 9F from OB sections ipilateral to the olfactory peduncle lesion). On average, 92% of GFP-ir cells in the GL express CB. On the contrary, only 53% of CB+ cells are GFP-ir. In addition, we also determined the percent overlap for GFP-ir cells in the EPL, MCL and IPL. Detailed information is listed in table 3. Interestingly, there are 3.2 and 4.3 times more GFP-ir cells than the CB+ cells in the EPL/MCL/IPL and GCL, respectively. Also the percents of GFP-ir cells expressing CB in these layers are much lower as compared to the GL (18.2%, and 3.6, respectively) (n=5 bulbs from 5 mice). Our data are consistent with the notion that CB expression likely depends on cellular function and is not cell type specific (Baimbridge et al., 1992, Cote and Parent, 1992). These results provide characterization of the chemical expression in these cholinergic interneurons in the OB and reveal the neurotransmitter identity for a subset of CB+ cells.

Discussion

Cholinergic interneurons are widely distributed in the central nervous system and play an essential role in brain functions (Woolf, 1991, Krnjevic, 1993). Here, we provide unambiguous and quantitative evidence showing the presence of a significant number of intrinsic cholinergic interneurons in the MOB of mice and that these neurons are diverse in distribution and morphological features. We also demonstrate that the cholinergic population partially overlaps with the CB+ population but is distinct from glutamatergic, doparminergic, GABAergic or CR+ interneuron populations. Additionally, we provide quantitative measurements of the cholinergic fiber density throughout the MOB and

VAChT-ir intensity in the GL. Together, our results provide the first relatively comprehensive view of the bulbar intrinsic cholinergic interneuron network and strongly suggest that olfactory activities in the MOB are modulated by both local and centrifugal cholinergic systems.

Location and morphological features of intrinsic cholinergic interneurons

Spatial distribution and synaptic connections of OB interneurons are key elements determining their physiological functions (Lledo et al., 2004; Shipley et al., 2004; Kosaka and Kosaka, 2005; Bovetti et al., 2007; Acebes et al., 2011). In our study, the largest population of intrinsic cholinergic interneurons is found within a the GL. Based on the observation that most of these GFP-ir cells arborize their nerve processes in single glomerulus, we consider they are PG cells. A few of the GFP-ir cells in the GL are considered JG cells because their processes extend into more than one glomerulus. These considerations are supported by our finding that 92% of these GFP-ir cells are CB-ir because CB is a well-known marker for a subset of PG interneurons (Toida et al., 1998). In addition, Toida et al. (1998) reported that CB+ cells form extensive dendrodendritic connections and rarely make direct synapses with axon terminals within glomeruli. Consistently, we found that nerve processes from GFP-ir cholinergic interneurons were more prevalent in non-ON zones lacking OMP or VGluT2 immunoreactivity. Future experiments are needed to determine the exact sites where these cholinergic interneurons modulate the signal processing within glomeruli.

The cholinergic neurons in the EPL, MCL, IPL and GCL are more diverse than those in the GL layer, especially those in the deep EPL, as their nerve processes can either arborize locally or travel for long distances in different directions. Clearly, the GFP-ir interneurons are not mitral/tufted cells, as they do not share similar morphology or the cell marker expression. Our study is consistent with Phelps et al (1992), which shows various local interneurons in the OB and higher-order olfactory cortices are labeled with an anti-ChAT antibody. Some of the interneurons reported in their study are similar to what we have seen in this study, such as those in the EPL possessing long nerve processes (Fig. 5G and H) and in the GCL (Fig. 5N). However, Phelps et al (1992) only showed a very limited number of OB cholinergic interneurons and, for most of them, only cell bodies and major nerve processes were presented. In our study, using the combination of transgenic marking and ChAT and VAChT immunolabeling, we are able to identify a significant number of cholinergic interneurons in the OB as well as reveal their diverse morphological features, especially fine nerve processes. Thus, our study presents a much detailed view on the diversity and complexity of the local cholinergic interneuron network in the mouse MOB.

Number of intrinsic cholinergic interneurons

We estimate 37,106+/-3706 cholinergic interneurons exist per MOB based on our cell counts and volume measurements. Using the ratios of GFP-ir over TH+ and CB+ cells, and the published estimation that about 6.35% and 5.81% of total cells per mouse bulb are TH+ and CB+, respectively (Parrish-Aungst et al., 2007), we estimate the cholinergic interneurons are about 4.1 to 4.8% of the total cells per bulb. Thus, the number of cholinergic interneurons is comparable with these interneurons and should be considered significant.

The discrepancy between our study and previous studies that show either no ChAT-ir cells (Butcher et al., 1992, Ichikawa et al., 1997) or only low and insignificant numbers (0.9 ChAT-immunoreactive cells in rat MOB/per 40μm-thick section (Ojima et al., 1988) is likely due to the methods used for visualizing these neurons. We demonstrated in our study that the intensity of ChAT-ir varies among brain cholinergic neurons and, in general, the

intensity in small-diameter cholinergic interneurons is weaker than that in the large-diameter cholinergic neurons (Fig. 1). We also demonstrated that intensity of ChAT-ir is influenced by the immunolabeling methods used. In our study, without antigen retrieval, the ChAT-ir in small-diameter cholinergic interneurons was often weak or even undetectable. These are consistent with the notion that low amounts of ChAT mRNA and protein present in the cell bodies may also contribute the difficulty in identifying local cholinergic interneurons (Wu and Hersh, 1994). However, some of these factors can surely be solved by using more sensitive methods as demonstrated by our study and by a previous study (Phelps et al., 1992). In their study, Phelps et al. focused on local interneurons in the OB and higher-order olfactory cortices and set criterion to ensure that these neurons were stained sufficiently well. In order to achieve this, they repeated the last two steps of immunohistochemical method (antibody-peroxidase-anti-peroxidase), which amplified the ChAT immunostaining intensity and allowed successful labeling of some local cholinergic interneurons in the rat OB and cortices. This approach of Phelps et al. (1992) is distinct from other studies that failed to label these neurons, many of which do not focus on the olfactory system or local cholinergic interneurons (Butcher et al., 1992, Ichikawa et al., 1997). Furthermore, we demonstrated the difficulty in identifying cholinergic cell bodies in the presence of extensive immunoreactive nerve fibers using either ChAT (Fig. 6B) or VAChT immunolabeling alone (Fig. 6G and I). Our results are also different from a recent study by (Salcedo et al., 2011), in which the authors mentioned very briefly that they found little evidence of local cholinergic interneurons in the mouse OB. However, they used a different transgenic mouse line. As described in the original paper characterizing the transgenic mice (Grybko et al., 2011), the tau-GFP is preferentially expressed in axons and only weak fluorescence was observed in cholinergic motor neurons. This is in distinct contrast to ChAT$^{(BAC)}$-eGFP mice that we used in our study where GFP fluorescence in cholinergic motor neurons is very bright (Tallini et al., 2006). Finally, differences in animal species or strains may also contribute to the discrepancy between studies. However, it is highly unlikely this is the main reason for the lack of local cholinergic interneurons in the OB since Phelps et al. (1992) successfully showed local cholinergic interneurons in the OB and olfactory cortices. More recent discoveries of local cholinergic interneurons in the fly antennal lobe further suggest that cholinergic interneurons may be a common and important subtype for olfactory information processing (Shang et al., 2007, Acebes et al., 2011).

Expression of chemospecific markers

Bulbar interneurons express various chemospecific markers and can be divided into many chemotypes accordingly (Shipley et al., 2004, Parrish-Aungst et al., 2007, Kosaka and Kosaka, 2011). We found that cholinergic cells did not immunoreact to antibodies specific for GABAergic, glutamatergic, dopaminergic or CR+ interneurons. Interestingly, the cholinergic population overlapped with the CB+ population, especially in the GL. Previously, Parrish-Aungest et al (2007) estimated about 65% of CB+ cells are GABAergic, and the remaining 35% had an unknown identity of neurotransmitter. Since we did not observe any cholinergic cells labeled with antibodies against either GABA or GAD65/67, the higher percentage of CB+ cholinergic (59% in our study vs 35%) is likely due to differences in tissue preparation and counting methods. CB is known to be expressed in distinct populations of brain neurons including those using GABA or ACh as neurotransmitters (Cote and Parent, 1992). Our identification that a subset of bulbar CB+ cells is cholinergic provides insight into the cholinergic activity and function of this subset of PG cells. Further studies are needed to elucidate the synaptic connection and physiological function of these cholinergic PG cells. Similar to those in the GL, cholinergic cells in the EPL, MCL and IPL did not express markers for dopaminergic, GABAergic, glutamatergic or CR+ cells. Also, only about 18% of them are CB+. Thus, the cholinergic

interneurons in the EPL/MCL/IPL form a distinct chemotype and may have different roles and postsynaptic partners.

Similarity and differences between intrinsic and centrifugal cholinergic systems

From our line intensity scan data, the intensity of VAChT-ir is significantly higher in glomerular neuropiles as compared to PG regions, suggesting that the neuropiles are the primary sites for cholinergic modulation from both cholinergic intrinsic interneurons and centrifugal nerve fibers. It has been reported that the cholinergic agonist, carbachol, when applied to glomeruli, changes the level of tonic presynaptic inhibition (Wachowiak et al., 2009). Also in the fly, local cholinergic neurons in the GL form excitatory local circuits and modulate the tuning property of output neurons (Shang et al., 2007). Interestingly, we also found that cholinergic nerve fibers are distributed primarily in non-ON zones (Fig. 2F and G, Fig. 4C). However, there are clear differences between the local interneuron network and centrifugal projection systems. Most of the intrinsic cholinergic interneurons are PG cells and exert local effects within single glomeruli in the GL, whereas centrifugal fibers are seen passing through many glomeruli. Whether these fibers modulate activity of multiple glomeruli has not been determined.

Based on our observation of their diverse distribution and arborization patterns, the local cholinergic interneurons, with their cell bodies primarily located in the deep EPL, MCL and IPL, can act either locally or across long distances. It is known that the secondary dendrites of mitral cells form dendrodendritic reciprocal synapses with dendrites of granule cells in the deep EPL. These synapses are essential for processing olfactory information and modulating mitral and tufted cell output (Mori et al., 1983, Greer, 1987, Isaacson and Strowbridge, 1998, Egger and Urban, 2006). The dendrodendritic synapses are subject to cholinergic modulation, which enhances neural and perceptual odor discrimination (Elaagouby et al., 1991, Tsuno et al., 2008, Ghatpande and Gelperin, 2009). Most likely, both centrifugal and local cholinergic interneurons contribute to this important modulation. Interestingly, we found that the number of cholinergic interneurons is 3.8 and 3.2 times more than the number of DA and CB interneurons, respectively in the deep EPL, MCL and IPL regions, which may reflect the importance of local cholinergic activity.

In our study, we find centrifugal projection nerve fibers in the IPL are strongly labeled with the VAChT antibody. We speculate that these fibers modulate OB activity on a large scale. It is known that cholinergic modulation enhances olfactory signals and filters trivial information based on memory, attention and expectation (Nickell and Shipley, 1993, Wilson et al., 2004, Fletcher and Chen, 2010). Future experiments using electron microscopy will be needed to determine whether individual centrifugal fibers make multiple synaptic contacts with many nerve processes.

Conclusions

We have found and characterized a significant number of intrinsic cholinergic interneurons in the mouse OB. Their diverse distribution and morphological features indicate the complexity of the local cholinergic network and its role in modulating olfactory activities. Likely, these cholinergic interneurons connect to different microcircuits and exert cholinergic influence on different postsynaptic partners. Thus, in our opinion, olfactory activities in the MOB are modulated by dual cholinergic systems made up by the local interneuron network and the centrifugal projection fibers. In future studies, it will be interesting to determine the differential and/or synergistic effects of centrifugal and intrinsic cholinergic regulation in the OB.

Acknowledgments

We thank Dr. M.I. Kotlikoff for providing us original mouse breeder pairs. This work was supported by NIH/NIDCD 009269 and ARRA administrative supplement to WL.

References

Acebes A, Martín-Peña A, Chevalier V, Ferrús A. Synapse loss in olfactory local interneurons modifies perception. The Journal of neuroscience. 2011; 31:2734–2745. [PubMed: 21414896]

Arvidsson U, Riedl M, Elde R, Meister B. Vesicular acetylcholine transporter (VAChT) protein: a novel and unique marker for cholinergic neurons in the central and peripheral nervous systems. The Journal of comparative neurology. 1997; 378:454–467. [PubMed: 9034903]

Aungst JL, Heyward PM, Puche AC, Karnup SV, Hayar A, Szabo G, Shipley MT. Centre-surround inhibition among olfactory bulb glomeruli. Nature. 2003; 426:623–629. [PubMed: 14668854]

Baimbridge KG, Celio MR, Rogers JH. Calcium-binding proteins in the nervous system. Trends in neurosciences. 1992; 15:303–308. [PubMed: 1384200]

Baker H, Kawano T, Margolis FL, Joh TH. Transneuronal regulation of tyrosine hydroxylase expression in olfactory bulb of mouse and rat. The Journal of neuroscience. 1983; 3:69–78. [PubMed: 6130133]

Bovetti S, Peretto P, Fasolo A, De Marchis S. Spatio-temporal specification of olfactory bulb interneurons. Journal of molecular histology. 2007; 38:563–569. [PubMed: 17588153]

Buck LB. Information coding in the vertebrate olfactory system. Annu Rev Neurosci. 1996; 19:517–544. [PubMed: 8833453]

Butcher LL, Oh JD, Woolf NJ, Edwards RH, Roghani A. Organization of central cholinergic neurons revealed by combined in situ hybridization histochemistry and choline-O-acetyltransferase immunocytochemistry. Neurochemistry international. 1992; 21:429–445. [PubMed: 1303168]

Carey RM, Verhagen JV, Wesson DW, Pirez N, Wachowiak M. Temporal structure of receptor neuron input to the olfactory bulb imaged in behaving rats. Journal of neurophysiology. 2009; 101:1073–1088. [PubMed: 19091924]

Carson KA. Localization of acetylcholinesterase-positive neurons projecting to the mouse main olfactory bulb. Brain research bulletin. 1984; 12:635–639. [PubMed: 6206927]

Castillo PE, Carleton A, Vincent JD, Lledó PM. Multiple and opposing roles of cholinergic transmission in the main olfactory bulb. The Journal of neuroscience. 1999; 19:9180–9191. [PubMed: 10531421]

Cave JW, Baker H. Dopamine systems in the forebrain. Adv Exp Med Biol. 2009; 651:15–35. [PubMed: 19731547]

Cote PY, Parent A. Calbindin D-28k and choline acetyltransferase are expressed by different neuronal populations in pedunculopontine nucleus but not in nucleus basalis in squirrel monkeys. Brain research. 1992; 593:245–252. [PubMed: 1450931]

Crespo C, Alonso JR, Briñón JG, Weruaga E, Porteros A, Arévalo R, Aijón J. Calcium-binding proteins in the periglomerular region of typical and typical olfactory glomeruli. Brain research. 1997; 745:293–302. [PubMed: 9037421]

Crespo C, Briñón JG, Porteros A, Arévalo R, Rico B, Aijón J, Alonso JR. Distribution of acetylcholinesterase and choline acetyltransferase in the main and accessory olfactory bulbs of the hedgehog (Erinaceus europaeus). The Journal of comparative neurology. 1999; 403:53–67. [PubMed: 10075443]

Crespo C, Porteros A, Arévalo R, Briñón JG, Aijón J, Alonso JR. Segregated distribution of nitric oxide synthase-positive cells in the periglomerular region of typical and atypical olfactory glomeruli. Neuroscience letters. 1996; 205:149–152. [PubMed: 8852580]

Doty RL, Bagla R, Kim N. Physostigmine enhances performance on an odor mixture discrimination test. Physiology & behavior. 1999; 65:801–804. PMID:10073483. [PubMed: 10073483]

Egger V, Urban NN. Dynamic connectivity in the mitral cell-granule cell microcircuit. Seminars in cell & developmental biology. 2006; 17:424–432. PMID:16889994. [PubMed: 16889994]

El-Etri MM, Ennis M, Griff ER, Shipley MT. Evidence for cholinergic regulation of basal norepinephrine release in the rat olfactory bulb. Neuroscience. 1999; 93:611–617. [PubMed: 10465445]

Elaagouby A, Ravel N, Gervais R. Cholinergic modulation of excitability in the rat olfactory bulb: effect of local application of cholinergic agents on evoked field potentials. Neuroscience. 1991; 45:653–662. [PubMed: 1775240]

Fletcher ML, Chen WR. Neural correlates of olfactory learning: Critical role of centrifugal neuromodulation. Learn Mem. 2010; 17:561–570. [PubMed: 20980444]

Frazier LL, Brunjes PC. Unilateral odor deprivation: early postnatal changes in olfactory bulb cell density and number. The Journal of comparative neurology. 1988; 269:355–370. [PubMed: 3372719]

Ghatpande AS, Gelperin A. Presynaptic muscarinic receptors enhance glutamate release at the mitral/tufted to granule cell dendrodendritic synapse in the rat main olfactory bulb. Journal of neurophysiology. 2009; 101:2052–2061. [PubMed: 19225175]

Godfrey DA, Ross CD, Herrmann AD, Matschinsky FM. Distribution and derivation of cholinergic elements in the rat olfactory bulb. Neuroscience. 1980; 5:273–292. [PubMed: 7374942]

Gracia-Llanes FJ, Crespo C, Blasco-Ibáñez JM, Marqués-Marí AI, Martínez-Guijarro FJ. VIP-containing deep short-axon cells of the olfactory bulb innervate interneurons different from granule cells. The European journal of neuroscience. 2003; 18:1751–1763. [PubMed: 14622210]

Greer CA. Golgi analyses of dendritic organization among denervated olfactory bulb granule cells. The Journal of comparative neurology. 1987; 257:442–452. [PubMed: 2435770]

Grybko MJ, Hahm ET, Perrine W, Parnes JA, Chick WS, Sharma G, Finger TE, Vijayaraghavan S. A transgenic mouse model reveals fast nicotinic transmission in hippocampal pyramidal neurons. The European journal of neuroscience. 2011; 33:1786–1798. [PubMed: 21501254]

Hayar A, Karnup S, Ennis M, Shipley MT. External tufted cells: a major excitatory element that coordinates glomerular activity. The Journal of neuroscience. 2004; 24:6676–6685. [PubMed: 15282270]

Ichikawa T, Ajiki K, Matsuura J, Misawa H. Localization of two cholinergic markers, choline acetyltransferase and vesicular acetylcholine transporter in the central nervous system of the rat: in situ hybridization histochemistry and immunohistochemistry. Journal of chemical neuroanatomy. 1997; 13:23–39. [PubMed: 9271193]

Isaacson JS, Strowbridge BW. Olfactory reciprocal synapses: dendritic signaling in the CNS. Neuron. 1998; 20:749–761. [PubMed: 9581766]

Kasa P, Karcsu S, Kovacs I, Wolff JR. Cholinoceptive neurons without acetylcholinesterase activity and enzyme-positive neurons without cholinergic synaptic innervation are present in the main olfactory bulb of adult rat. Neuroscience. 1996; 73:831–844. [PubMed: 8809802]

Kiyokage E, Pan YZ, Shao Z, Kobayashi K, Szabo G, Yanagawa Y, Obata K, Okano H, Toida K, Puche AC, Shipley MT. Molecular identity of periglomerular and short axon cells. The Journal of neuroscience. 2010; 30:1185–1196. [PubMed: 20089927]

Kosaka K, Kosaka T. synaptic organization of the glomerulus in the main olfactory bulb: compartments of the glomerulus and heterogeneity of the periglomerular cells. Anatomical science international. 2005; 80:80–90. [PubMed: 15960313]

Kosaka T, Kosaka K. Heterogeneity of parvalbumin-containing neurons in the mouse main olfactory bulb, with special reference to short-axon cells and betaIV-spectrin positive dendritic segments. Neuroscience research. 2008; 60:56–72. [PubMed: 17976845]

Kosaka T, Kosaka K. Heterogeneity of calbindin-containing neurons in the mouse main olfactory bulb: I. General description. Neuroscience research. 2010; 67:275–292. [PubMed: 20406658]

Kosaka T, Kosaka K. “Interneurons” in the olfactory bulb revisited. Neuroscience research. 2011; 69:93–99. [PubMed: 20955739]

Krasteva G, Canning BJ, Hartmann P, Veres TZ, Papadakis T, Muhlfeld C, Schliecker K, Tallini YN, Braun A, Hackstein H, Baal N, Weihe E, Schutz B, Kotlikoff M, Ibanez-Tallon I, Kummer W. Cholinergic chemosensory cells in the trachea regulate breathing. Proceedings of the National Academy of Sciences of the United States of America. 2011; 108:9478–9483. [PubMed: 21606356]

Krnjevic K. Central cholinergic mechanisms and function. Progress in brain research. 1993; 98:285–292. [PubMed: 8248518]

Le Jeune H, Jourdan F. Postnatal development of cholinergic markers in the rat olfactory bulb: a histochemical and immunocytochemical study. The Journal of comparative neurology. 1991; 314:383–395. [PubMed: 1787181]

Le Jeune H, Jourdan F. Acetylcholinesterase-containing intrinsic neurons in the rat main olfactory bulb: cytological and neurochemical features. The European journal of neuroscience. 1994; 6:1432–1444. [PubMed: 7528084]

Lin W, Ogura T, Margolskee RF, Finger TE, Restrepo D. TRPM5-expressing solitary chemosensory cells respond to odorous irritants. Journal of neurophysiology. 2008; 99:1451–1460. [PubMed: 18160424]

Lin W, Margolskee R, Donnert G, Hell SW, Restrepo D. Olfactory neurons expressing transient receptor potential channel M5 (TRPM5) are involved in sensing semiochemicals. Proc Natl Acad Sci USA. 2007; 104:2471–2476. [PubMed: 17267604]

Lledo PM, Saghatelyan A, Lemasson M. Inhibitory interneurons in the olfactory bulb: from development to function. Neuroscientist. 2004; 10:292–303. [PubMed: 15271257]

Macrides F, Davis BJ, Youngs WM, Nadi NS, Margolis FL. Cholinergic and catecholaminergic afferents to the olfactory bulb in the hamster: a neuroanatomical, biochemical, and histochemical investigation. The Journal of comparative neurology. 1981; 203:495–514. [PubMed: 6274923]

Matsutani S, Yamamoto N. Centrifugal innervation of the mammalian olfactory bulb. Anatomical science international. 2008; 83:218–227. [PubMed: 19159349]

Mechawar N, Descarries L. The cholinergic innervation develops early and rapidly in the rat cerebral cortex: a quantitative immunocytochemical study. Neuroscience. 2001; 108:555–567. [PubMed: 11738494]

Mori K, Kishi K, Ojima H. Distribution of dendrites of mitral, displaced mitral, tufted, and granule cells in the rabbit olfactory bulb. The Journal of comparative neurology. 1983; 219:339–355. [PubMed: 6619342]

Mori K, Nagao H, Yoshihara Y. The olfactory bulb: coding and processing of odor molecule information. Science. 1999; 286:711–715. [PubMed: 10531048]

Nakajima T, Murabayashi C, Ogawa K, Taniguchi K. Immunoreactivity of protein gene product 9.5 (PGP 9.5) in the developing hamster olfactory bulb. The Anatomical record. 1998; 250:238–244. [PubMed: 9489784]

Nickell WT, Shipley MT. Two anatomically specific classes of candidate cholinoceptive neurons in the rat olfactory bulb. The Journal of neuroscience. 1988; 8:4482–4491. [PubMed: 3199188]

Nickell WT, Shipley MT. Evidence for presynaptic inhibition of the olfactory commissural pathway by cholinergic agonists and stimulation of the nucleus of the diagonal band. The Journal of neuroscience. 1993; 13:650–659. [PubMed: 8426231]

Oda Y, Nakanishi I. The distribution of cholinergic neurons in the human central nervous system. Histology and histopathology. 2000; 15:825–834. [PubMed: 10963126]

Ogura T, Krosnowski K, Zhang L, Bekkerman M, Lin W. Chemoreception regulates chemical access to mouse vomeronasal organ: role of solitary chemosensory cells. PLoS One. 2010; 5:e11924. [PubMed: 20689832]

Ogura T, Margolskee RF, Tallini YN, Shui B, Kotlikoff MI, Lin W. Immuno-localization of vesicular acetylcholine transporter in mouse taste cells and adjacent nerve fibers: indication of acetylcholine release. Cell Tissue Res. 2007; 330:17–28. [PubMed: 17704949]

Ogura T, Szebenyi SA, Krosnowski K, Sathyanesan A, Jackson J, Lin W. Cholinergic microvillous cells in the mouse main olfactory epithelium and effect of acetylcholine on olfactory sensory neurons and supporting cells. Journal of neurophysiology. 2011; 106:1274–1287. [PubMed: 21676931]

Ojima H, Yamasaki T, Kojima H, Akashi A. Cholinergic innervation of the main and the accessory olfactory bulbs of the rat as revealed by a monoclonal antibody against choline acetyltransferase. Anatomy and embryology. 1988; 178:481–488. [PubMed: 3223607]

Parrish-Aungst S, Shipley MT, Erdelyi F, Szabo G, Puche AC. Quantitative analysis of neuronal diversity in the mouse olfactory bulb. The Journal of comparative neurology. 2007; 501:825–836. [PubMed: 17311323]

Phelps PE, Houser CR, Vaughn JE. Small cholinergic neurons within fields of cholinergic axons characterize olfactory-related regions of rat telencephalon. Neuroscience. 1992; 48:121–136. [PubMed: 1584418]

Pressler RT, Inoue T, Strowbridge BW. Muscarinic receptor activation modulates granule cell excitability and potentiates inhibition onto mitral cells in the rat olfactory bulb. The Journal of neuroscience. 2007; 27:10969–10981. [PubMed: 17928438]

Ravel N, Elaagouby A, Gervais R. Scopolamine injection into the olfactory bulb impairs short-term olfactory memory in rats. Behavioral neuroscience. 1994; 108:317–324. [PubMed: 8037875]

Rosen GD, Harry JD. Brain volume estimation from serial section measurements: a comparison of me thodologies. Journal of neuroscience methods. 1990; 35:115–124. [PubMed: 2283883]

Salcedo E, Tran T, Ly X, Lopez R, Barbica C, Restrepo D, Vijayaraghavan S. Activity-dependent changes in cholinergic innervation of the mouse olfactory bulb. PLoS One. 2011; 6:e25441. [PubMed: 22053179]

Sassoe-Pognetto M. Molecular and functional heterogeneity of neural circuits: an example from the olfactory bulb. Brain Res Rev. 2011; 66:35–42. [PubMed: 20600309]

Sathyanesan A, Ogura T, Lin W. Automated measurement of nerve fiber density using line intensity scan analysis. J Neurosci Methods. 2012; 206:165–175. http://dx.doi.org/10.1016/j.jneumeth.2012.02.019. [PubMed: 22613744]

Sato Y, Nakajima S, Shiraga N, Atsumi H, Yoshida S, Koller T, Gerig G, Kikinis R. Three-dimensional multi-scale line filter for segmentation and visualization of curvilinear structures in medical images. Medical image analysis. 1998; 2:143–168. [PubMed: 10646760]

Shang Y, Claridge-Chang A, Sjulson L, Pypaert M, Miesenbock G. Excitatory local circuits and their implications for olfactory processing in the fly antennal lobe. Cell. 2007; 128:601–612. [PubMed: 17289577]

Shao Z, Puche AC, Kiyokage E, Szabo G, Shipley MT. Two GABAergic intraglomerular circuits differentially regulate tonic and phasic presynaptic inhibition of olfactory nerve terminals. Journal of neurophysiology. 2009; 101:1988–2001. [PubMed: 19225171]

Shepherd, GM.; Chen, WR.; Greer, CA. Olfactory bulb.. In: Shepherd, GM., editor. The synaptic organization of the brain. 5th ed. Oxford; New York: 2004. p. 165-216.

Shinoda K, Ohtsuki T, Nagano M, Okumura T. A possible functional necklace formed by placental antigen X-P2-immunoreactive and intensely acetylcholinesterase-reactive (PAX/IAE) glomerular complexes in the rat olfactory bulb. Brain research. 1993; 618:160–166. [PubMed: 8402170]

Shipley, MT.; Ennis, M.; Puche, AC. Olfactory system.. In: Paxinos, G., editor. The rat nervous system. Academic Press; San Diego: 2004. p. 921-961.

Spors H, Wachowiak M, Cohen LB, Friedrich RW. Temporal dynamics and latency patterns of receptor neuron input to the olfactory bulb. The Journal of neuroscience. 2006; 26:1247–1259. [PubMed: 16436612]

Tallini YN, Shui B, Greene KS, Deng KY, Doran R, Fisher PJ, Zipfel W, Kotlikoff MI. BAC transgenic mice express enhanced green fluorescent protein in central and peripheral cholinergic neurons. Physiological genomics. 2006; 27:391–397. [PubMed: 16940431]

Toida K, Kosaka K, Heizmann CW, Kosaka T. Chemically defined neuron groups and their subpopulations in the glomerular layer of the rat main olfactory bulb: III. Structural features of calbindin D28K-immunoreactive neurons. The Journal of comparative neurology. 1998; 392:179–198. [PubMed: 9512268]

Tsuno Y, Kashiwadani H, Mori K. Behavioral state regulation of dendrodendritic synaptic inhibition in the olfactory bulb. The Journal of neuroscience. 2008; 28:9227–9238. [PubMed: 18784303]

Wachowiak M, Cohen LB. Representation of odorants by receptor neuron input to the mouse olfactory bulb. Neuron. 2001; 32:723–735. [PubMed: 11719211]

Wachowiak M, Shipley MT. Coding and synaptic processing of sensory information in the glomerular layer of the olfactory bulb. Seminars in cell & developmental biology. 2006; 17:411–423. PMID: 16765614. [PubMed: 16765614]

Wachowiak M, Wesson DW, Pirez N, Verhagen JV, Carey RM. Low-level mechanisms for processing odor information in the behaving animal. Annals of the New York Academy of Sciences. 2009; 1170:286–292. [PubMed: 19686149]

Weihe E, Tao-Cheng JH, Schafer MK, Erickson JD, Eiden LE. Visualization of the vesicular acetylcholine transporter in cholinergic nerve terminals and its targeting to a specific population of small synaptic vesicles. Proceedings of the National Academy of Sciences of the United States of America. 1996; 93:3547–3552. [PubMed: 8622973]

Wenk H, Meyer U, Bigl V. Centrifugal cholinergic connections in the olfactory system of rats. Neuroscience. 1977; 2:797–800. [PubMed: 593558]

Wilson DA, Fletcher ML, Sullivan RM. Acetylcholine and olfactory perceptual learning. Learn Mem. 2004; 11:28–34. [PubMed: 14747514]

Woolf NJ. Cholinergic systems in mammalian brain and spinal cord. Progress in neurobiology. 1991; 37:475–524. [PubMed: 1763188]

Wu D, Hersh LB. Choline acetyltransferase: celebrating its fiftieth year. Journal of neurochemistry. 1994; 62:1653–1663. [PubMed: 8158117]

Zaborszky L, Carlsen J, Brashear HR, Heimer L. Cholinergic and GABAergic afferents to the olfactory bulb in the rat with special emphasis on the projection neurons in the nucleus of the horizontal limb of the diagonal band. The Journal of comparative neurology. 1986; 243:488–509. [PubMed: 3512629]

Zheng LM, Ravel N, Jourdan F. Topography of centrifugal acetylcholinesterase-positive fibres in the olfactory bulb of the rat: evidence for original projections in atypical glomeruli. Neuroscience. 1987; 23:1083–1093. [PubMed: 3437990]

Highlights

We found a large number of cholinergic interneurons in the mouse olfactory bulb.

These interneurons express cholinergic marker ChAT and VAChT.

They exhibit diverse morphological features and distribution patterns.

They are distinct from glutamatergic, GABAergic or dopaminergic interneurons.

Intrinsic cholinergic interneurons likely play diverse roles in olfactory processing.

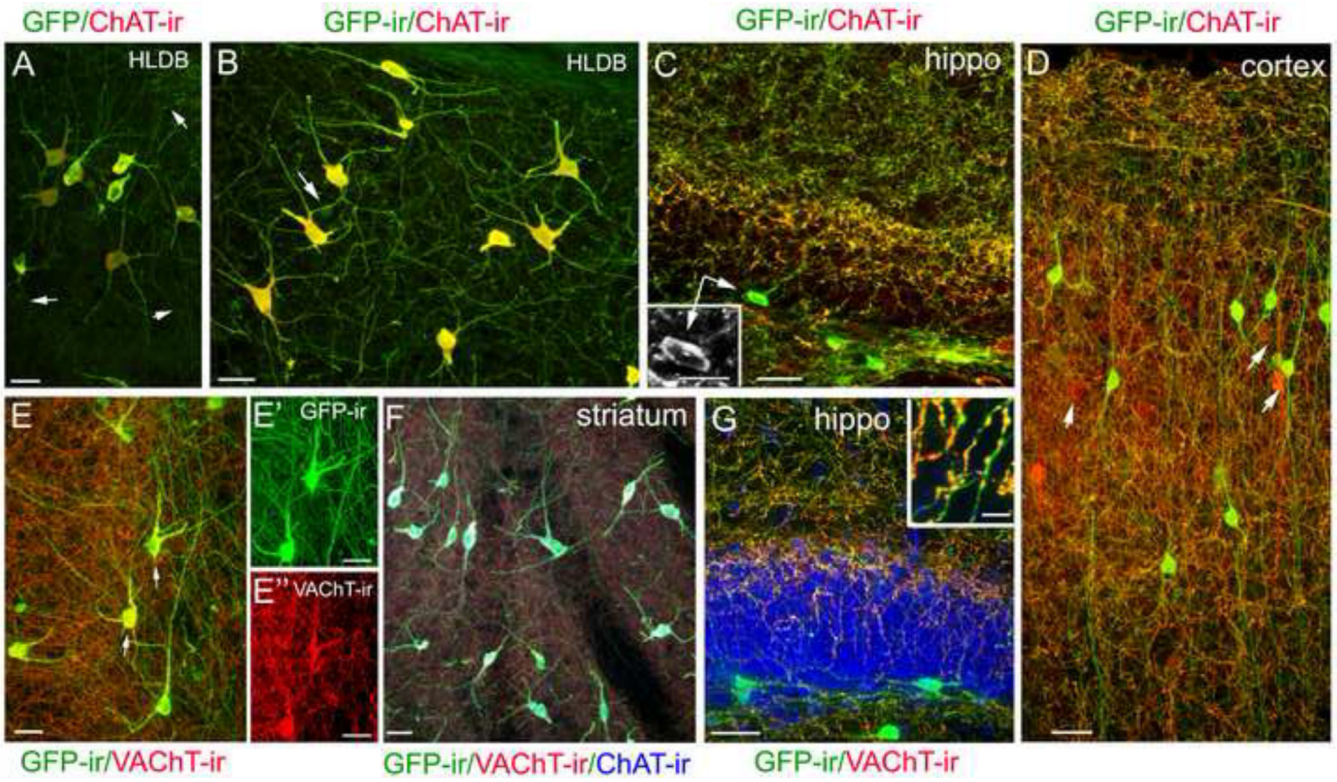

Figure 1. Immunoreactivity of ChAT and VAChT in brain GFP-expressing neurons of ChAT$^{(BAC)}$-GFP mice

A: A representative confocal image showing GFP-fluoresecence and ChAT-ir (red) in large-diameter neurons of the horizontal limb of the diagonal band of Broca (HLDB). Both GFP flourescence and ChAT-ir are intense in cell bodies and proximal regions of their processes. In the distal regions, the signals are relatively weak and ChAT-ir is sometimes undetectable (pointed by arrows). B: A representative confocal image of a population of neurons taken from a similar region of A, showing that both GFP signal and ChAT-ir are enhanced by an anti-GFP antibody and antigen retrieval treatment, respectively. Arrow points a small-diameter neuron with relatively weak GFP-ir. C: A representative confocal image of GFP-ir and ChAT-ir in the hippocampus (hippo) showing both cholinergic network and interneurons. Inset shows ChAT-ir in the soma of a GFP-ir interneurons (arrows). D: GFP-ir and ChAT-ir in the cortex showing local cholinergic interneurons, the nerve processes and the vast cholinergic network. ChAT-ir is present in cell bodies of the GFP-ir interneurons although ChAT-ir is generally weak or undetectable in their nerve processes, , in contrast to the vast cholinergic network where ChAT-ir is strong and highly colocalized with GFP-ir. Arrow points few cells that exhibit strong ChAT-ir with weak or undetectable GFP-ir. E: A typical image of VAChT-ir (red) in GFP-ir neurons and processes. Strong VAChT-ir is co-localized in cell bodies of large-diameter neurons and numerous fine nerve processes in the network but less intense or absent in some thick GFP-ir fibers. This image was taken from a region immediately posterior to the anterior commissure. Arrows point to two cells that are presented in E' and E" showing individual images of GFP-ir and VAChT-ir, respectively. F: Colocalization of GFP, VAChT-ir (red) and ChAT-ir (blue) in large-diameter neurons. G: VAChT-ir is present in hippocampal GFP+ nerve fibers but is absent in the cell bodies. Inset: Enlarged image from G showing VAChT-ir in varicose structures of GFP-ir nerve fibers. Scale: 20 μm.

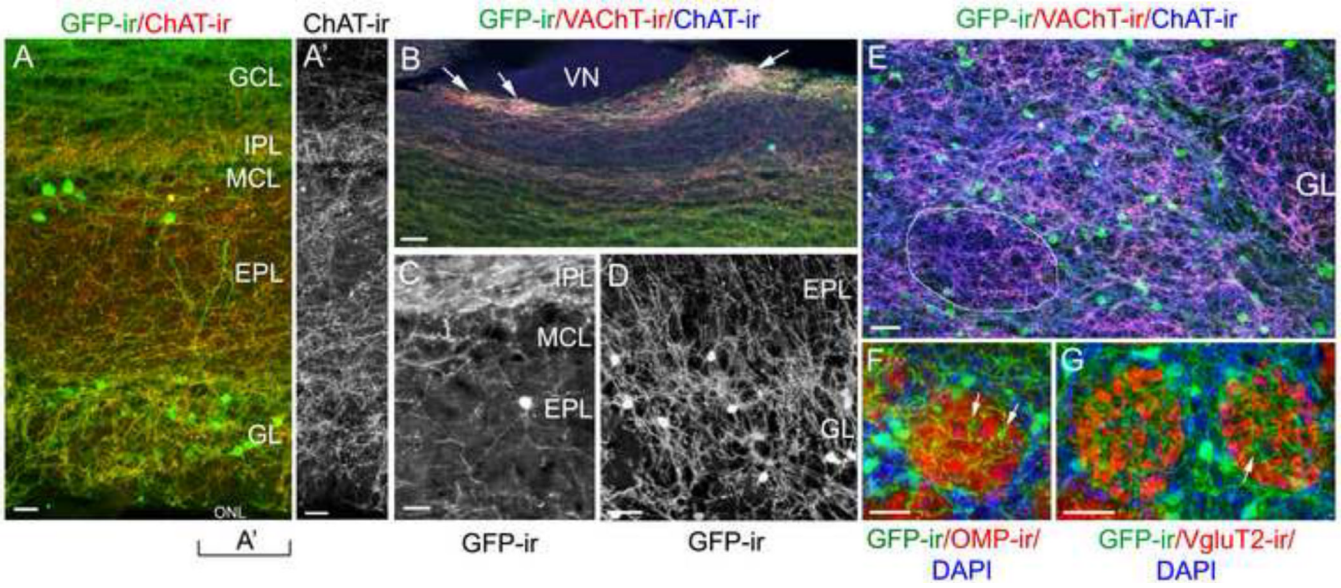

Figure 2. Cholinergic nerve processes in the OB visualized by GFP, ChAT and VAChT immunoreactivity

A: A low magnification confocal image of typical GFP-ir and ChAT-ir (red) in various layers of the OB. GCL: granule cell layer. IPL: internal plexiform layer. MCL: mitral cell layer. EPL: external plexiform layer. GL: glomerular layer. ONL: olfactory nerve layer. Numerous nerve fibers in the GL, EPL, IPL and GCL are positive for GFP-ir and ChAT-ir. Note the labeled interneuron cell bodies in the GL and EPL. A': Image of ChAT-ir alone from the left region of panel A. B: A confocal image of a caudal region of the MOB showing colocalization of GFP-ir, ChAT-ir and VAChT-ir in nerve fibers (green, blue and red, respectively). Three atypical glomeruli receive dense cholinergic innervation (pointed by arrows). VN: vomeronasal nerve. C: A representative confocal image showing some GFP-ir fibers exit the IPL and travel through the MCL to the EPL. Note a GFP-ir interneuron in the mid-EPL. D: A typical image of the superficial EPL and GL showing GFP-ir nerve fibers in these layers. GFP-ir fibers are present within and surrounding glomeruli and travel between the EPL and GL in their border region. Images of C and D were taken from 25 μm-thick OB sections. E: A patch of glomeruli from a medial sagittal section labeled with both ChAT and VAChT antibodies. VAChT-ir (red) and ChAT-ir (blue) are intense in the glomerular neuropiles as compared to the surrounding PG regions. A representative glomerulus is circled. F and G: Glomeruli labeled with antibodies against OMP or VGluT2, respectively (red). Within the glomeruli GFP-ir fibers are primarily located in sub-compartments lacking OMP-ir and VGluT2-ir. Arrows point to a small GFP-ir fiber plexus. Note the presence of many GFP-ir PG interneurons, which we quantify in Table 2. Scale: A, 50μm. B through G, 25 μm.

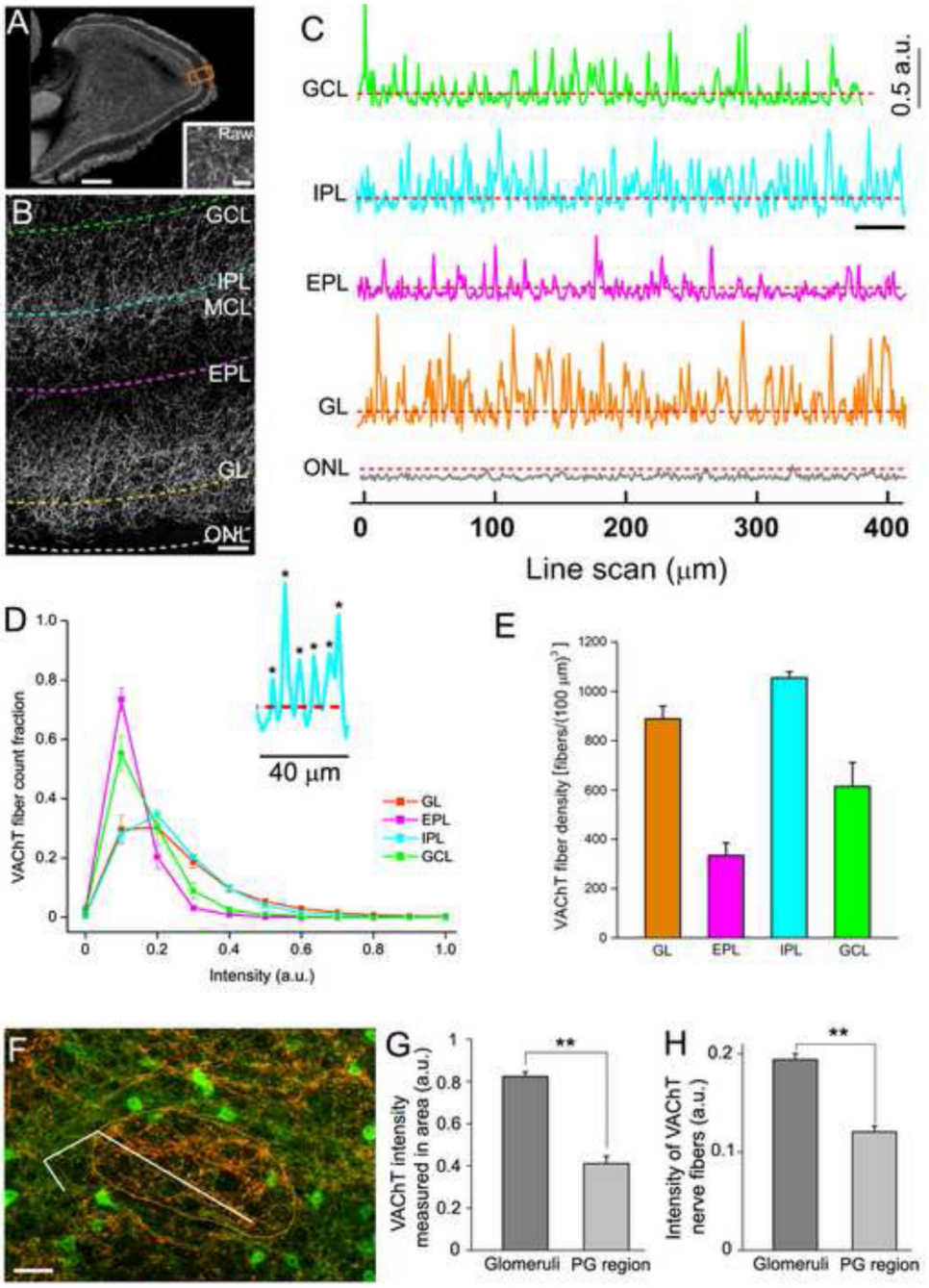

Figure 3. Quantitative measurement of cholinergic fiber density in olfactory bulb layers

A: A representative epifluorescence image of VAChT-ir in a sagittal OB section used for fiber density measurement. The image was taken using a 4X objective lens and processed using Hessian based feature extraction in ImageJ (Sathyanesan et al 2012). Inset shows a raw image (Raw) from an EPL region before Hessian feature extraction. Line-intensity scans were conducted in all layers. The orange rectangle indicates the relative size of the image in panel B. B: An enlarged Hessian extracted image showing VAChT-ir in different layers. Individual dashed lines denote parallel line intensity scans in these layers. Perpendicular line scans are not indicated in this image. C: Line intensity profiles of VAChT-immunolabeled nerve fibers corresponding to fluorescence intensity along the dashed lines in B. Each scan

starts from left to right. Each hit of these nerve fibers is shown as an intensity peak in the scan. a.u.: arbitrary unit of fluorescence intensity. All line scan profiles were baseline corrected (Sathyanesan et al., 2012). D: Histogram of intensity distribution for VAChT-immunolabeled nerve fibers in various layers from parallel scans conducted on images of entire sagittal OB sections similar to panel A. Average parallel scan lengths per bulb were 26.3 mm (GL), 23.9 mm (EPL), 20.5 mm (IPL), 18.3 mm (GCL) (n = three bulbs from three mice). More VAChT labeled nerve fibers in the IPL and GL show relatively higher intensity values, whereas a higher fraction (~80%) of the nerve fibers counted in the EPL show relatively low intensity value. Inset: Enlarged line intensity profile from the underlined portion of the IPL scan profile. Each peak indicates a nerve fiber detected by the line scan (marked by asterisks). E: Average density plot of VAChT-immunolabeled nerve fibers for individual layers on the entire OB sections. Fiber density was calculated per volume based on (1) parallel line scans and 5 additional line scans perpendicular to the parallel scans conducted in each layer and (2) the thickness of the sections. F: A glomerulus from a medial sagittal section labeled with the VAChT antibody (circled by the orange line). The segmented line through both the glomerular neuropile and the periglomerular region denotes the line intensity scan used to measure the VAChT-ir intensity of individual nerve fibers. G: Average VAChT-ir intensity in glomerular neuropiles and PG regions (n=10 and 6, respectively). H: Average VAChT-ir intensity in individual nerve fibers within glomeruli or PG regions from line intensity scan through 20 glomeruli and 10 PG regions, respectively. VAChT-ir is significantly higher in the neuropiles than in PG regions ($p < 0.01$). Scale: A, 1mm. Inset in A, 25 μm. B, 50μm. G, 20 μm.

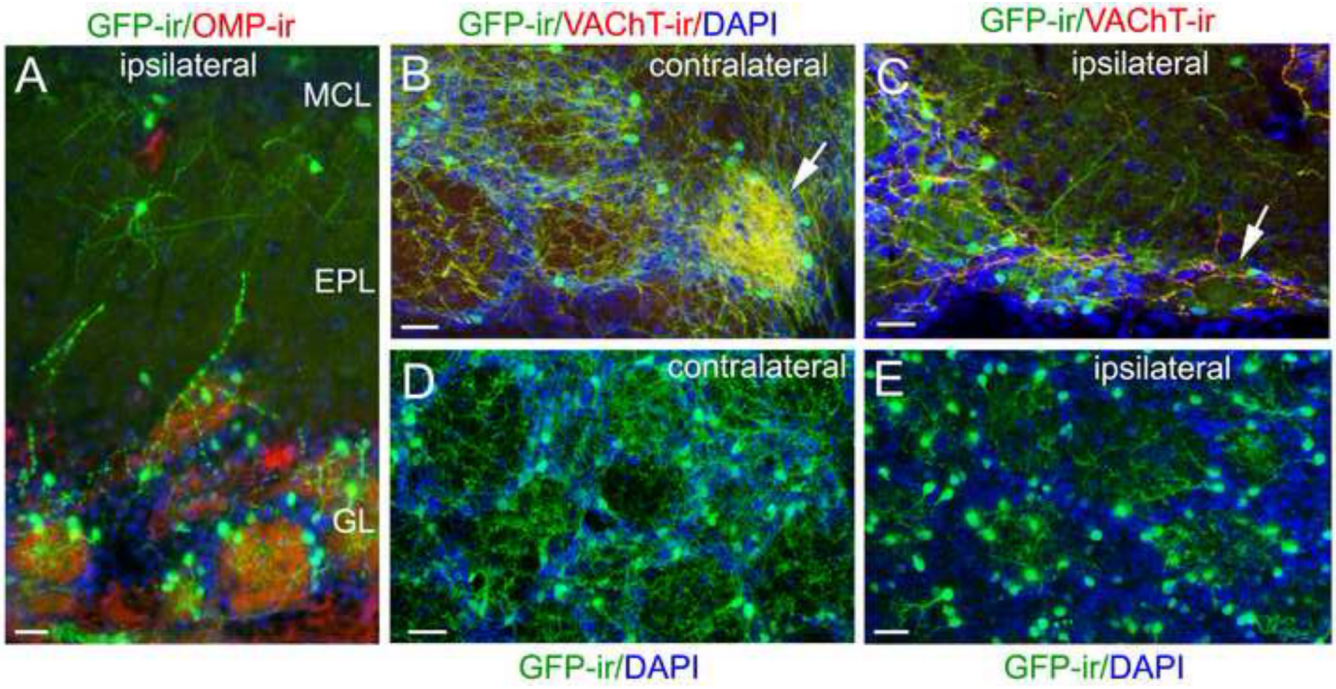

Figure 4. Ipsilateral olfactory peduncle lesion diminishes centrifugal cholinergic projections, allowing a better view of the intrinsic cholinergic system

A: A representative confocal image of local cholinergic cells and nerve processes in the MCL, EPL and GL after surgery. The OB section was immunolabeled with the anti-OMP (red) and anti-GFP (green) antibodies and counterstained with DAPI (blue). GFP-ir centrifugal fibers in these layers are diminished, but there are many GFP-ir interneurons in the GL and some in the EPL and MCL. B: A confocal image of GFP-ir and VAChT-ir from a caudal-ventral OB region contralateral to the lesion, showing both several typical glomeruli and an atypical glomerulus, which receives dense cholinergic innervation (pointed by an arrow). C: Ipsilateral bulb section showing similar area of B. The dense cholinergic innervation in the atypical glomerulus was lost (pointed by an arrow). D: An representative image taken from a medial sagittal OB section contralateral to the lesion site, showing a patch of glomeruli. Individual glomeruli are outlined by DAPI staining (blue). There are numerous GFP-ir fibers within glomeruli and in surrounding regions. E: A representative image taken from an OB section ispilateral to the lesion site. DAPI nuclear staining (blue) outlines individual glomeruli. Note that GFP-ir fibers surrounding individual glomeruli are diminished. However, within the glomeruli there are many nerve processes that clearly emanate from local GFP-ir interneurons in the GL. Scale: 25 μm.

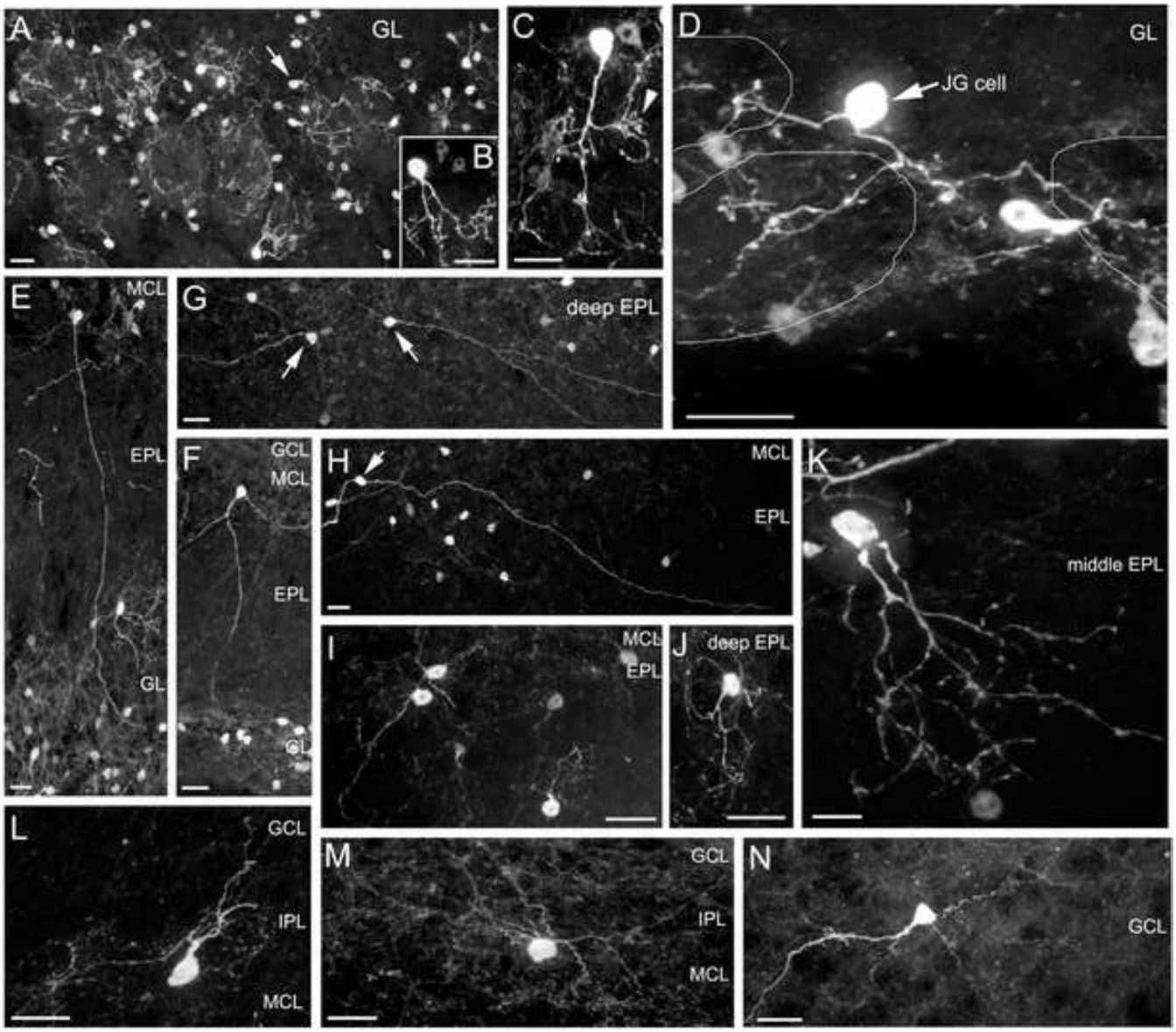

Figure 5. Intrinsic cholinergic interneurons in the OB are diverse in morphology and distribution

All images are from OB sections ipsilateral to olfactory peduncle lesion, representing the major morpholigical subtypes in various layers. A to D: GFP-ir cholinergic interneurons in the GL. A: A patch of glomeruli showing that most of the GFP-ir cells are PG cells with primary processes arborizing in a single glomerulus. Few of the GFP-ir interneurons are considered as JG cells, which send processes to more than one glomerulus. An arrow points to a JG cell. B and C: Examples of individual GFP-ir PG cells. An arrowhead points to a small region where a fiber arborizes extensively. D: A JG cell with two major processes that branch and innervate three individual glomeruli outlined by thin lines. E to K: GFP-ir cholinergic interneurons in the EPL. The anatomical locations of various layers are indicated. E and F: Two interneurons, whose cell bodies reside in the deep EPL, project their primary processes to the GL. G and H: GFP-ir interneurons (pointed by arrows) in the deep EPL with two main processes protruding often from opposite ends of the cell bodies. Their primary processes travel for long distances usually in the deep EPL and in parallel to the

MCL. I and J: GFP-ir interneurons in the MCL and deep EPL with multiple short and fine processes. K: A GFP-ir cell in the middle EPL. L and M: Two GFP-ir cells in the IPL. The cell in panel M apparently does not have a primary process. N: A GFP-ir cell in the GCL showing many spine-like structures. Scale: 20 μm.

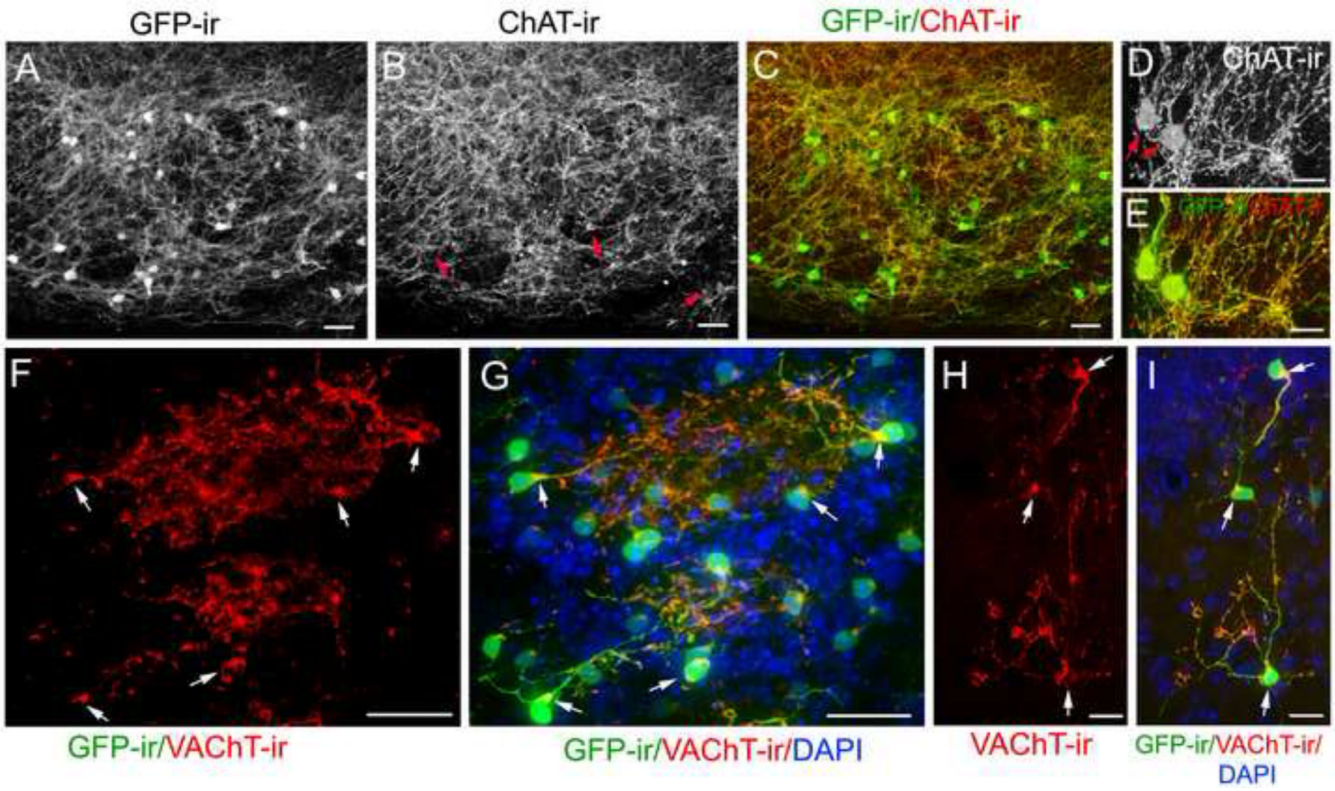

Figure 6. ChAT and VAChT immunoreactivity in bulbar interneurons

A: A typical confocal image showing substantial GFP-ir fibers and many cell bodies of interneurons in the GL. B: Image of ChAT-ir in the same region of A showing asimilar labeling pattern to GFP-ir. Both cholinergic nerve fibers and cell bodies are positive for ChAT-ir. Representative cell bodies are pointed by arrows. These cell bodies are difficult to recognize in the presence of the extensive ChAT-ir fiber network. C: Image of A overlaid onto B, showing that the GFP-ir is colocalized with ChAT-ir in both nerve fibers and interneuron cell bodies. D: A high magnification confocal image, showing ChAT-ir in two cell bodies as well as nerve processes. E: The GFP-ir image overlaid onto D, showing colocalization of GFP-ir and ChAT-ir. F to I contains images from OB sections ipsilateral to the olfactory peduncle lesion. F: A representative VAChT-ir image taken from the GL. Strong VAChT-ir is observed in nerve processes within the glomeruli. The cell bodies emanating these nerve processes are also labeled. Note that VAChT-ir in the cell bodies is primarily located only in small regions from which the primary processes protrude. A few representative cell bodies are pointed by arrows. G: The GFP-ir image overlaid onto F, showing colocalization of these two signals. DAPI counterstain: blue. H: A representative image showing four VAChT-immunolabeled local cholinergic interneurons with cell bodies residing in the EPL (bottom, middle right), MCL (middle, left) and IPL (top). I: The GFP image overlaid onto H. DAPI counterstain: blue. Scale: A to C, F and G, 25μm. D, E, H and I, 10 μm.

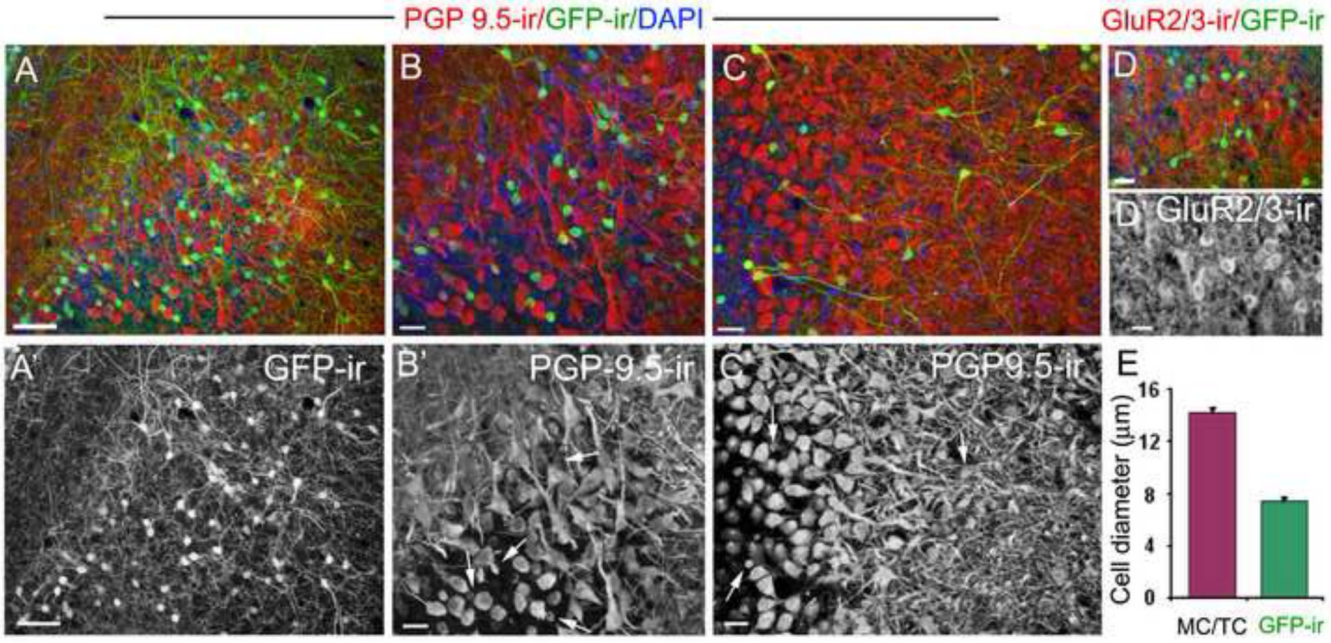

Figure 7. The cholinergic (GFP-ir) interneurons in the mitral cell layer are not mitral/tufted cells

A: A representative image of GFP-ir and PGP 9.5 immunoreactivity (PGP9.5-ir) in the EPL and MCL. The PGP 9.5 antibody strongly labeled mitral/tufted cells and their nerve processes (red), as well as GFP-ir cell bodies. A': Image of GFP-ir alone. B and B': An enlarged image showing the MCL region in panel A (lower middle portion) and PGP9.5-ir alone, respectively. The GFP-ir signal (green) in panel B is reduced using Adobe Photoshop for better visualization of the cell bodies. The GFP-ir cells exhibit smaller cell bodies and thin nerve processes, whereas mitral cells are multi-polar with large cell bodies and thick nerve processes. None of the mitral cells are positive for GFP-ir. C and C': Cholinergic interneurons (GFP-ir) and PGP9.5-labeled mitral/tufted cells viewed from a different angle. GFP-ir cell bodies in the deep EPL and the MCL intermingle with mitral/tufted cell bodies and processes. Some GFP-ir cells show long nerve processes. Representative GFP-ir cell bodies are pointed by arrows in B' and C'. D: A representative confocal image of GluR2/3 immunoreactivity (GluR2/3-ir) in mitral/tufted cells and GFP-ir. D': GluR2/3-ir alone. Stronger GluR2/3-ir is seen in cell bodies as compared to the surrounding nerve processes. There is no colocalization between GFP-ir and GluR2/3-ir. DAPI (blue) in A, B, C and D. E: Average cell diameters measured from GFP-ir cells and cells labeled with PGP 9.5-ir or GluR2/3-ir. For mitral/tufted cells, only those with recognizable morphological features were measured (22 cells for each group, respectively). Scale: A, 50μm. B to E, 20μm.

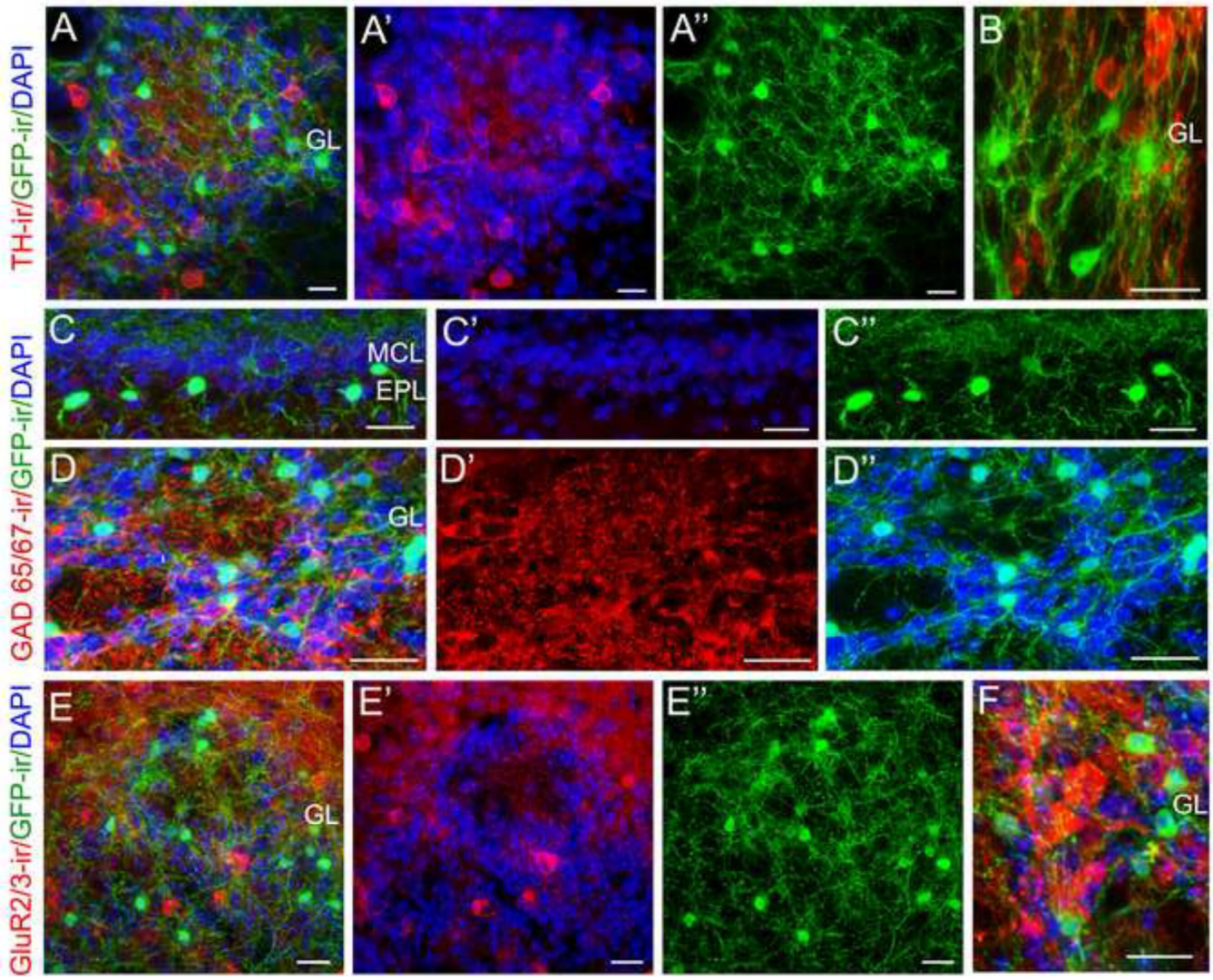

Figure 8. The GFP-expressing cholinergic interneurons are distinct from dopaminergic, GABAergic or glutamatergic interneurons

A: A representative confocal image showing TH immunoreactivity (TH-ir, red), GFP-ir (green) and DAPI (blue) within a glomerulus and surrounding PG interneurons. A': Image of TH-ir with DAPI outlining the glomerulus. A": Image of GFP-ir. B: TH-ir and GFP-ir shown at a higher magnification. TH-ir is present in many interneurons and nerve processes, none of which are GFP-ir positive. C and D: Representative images showing GAD65/67 immunoreactivity (GAD65/67-ir, red), GFP-ir and DAPI in the EPL and the GL, respectively. C': Image of GAD65/67-ir with packed DAPI-stained nuclei marking the MCL. C": Image of GFP-ir in the EPL. D': Image of GAD65/67-ir PG interneurons and their processes in the GL. D": Image of GFP-ir and DAPI staining, which outlines the glomeruli. Note GFP-ir and GAD65/67-ir are present in two distinct populations of interneurons. E: A representative image of GluR 2/3-ir (red), GFP-ir and DAPI. E': GluR 2/3-ir with DAPI. E": image of GFP-ir alone. A subset of interneurons in the GL positively reacted to the antibody against the glutamatergic marker GluR 2/3 (red). None of the GFP-ir cells and processes are labeled. F: A higher magnification image of GAD65/67-ir (red) and GFP-ir. Scale: 20 μm.

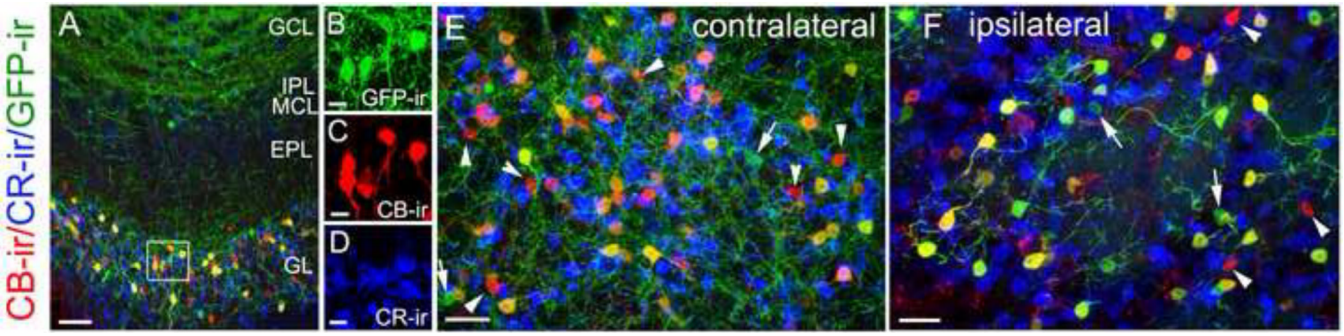

Figure 9. Expression of calcium binding proteins in bulbar cholinergic cells

A: Low magnification image showing GFP-ir (green), CB and CR immunoreactivity (CB-ir and CR-ir, red and blue, respectively) in various layers of the OB. Most of the CB or CR immuoreactive interneurons are located in the GL. Some are found in the EPL. B, C and D: Enlarged images showing single labeling of GFP-ir, CB-ir and CR-ir, respectively, from the box region in the GL in panel A. E and F: High magnification images from the GL showing GFP-ir, CB-ir and CR-ir cells in OB sections either countralateral (B) or ipsilateral (C) to the olfactory peduncle lesion. CR and CB are expressed in two separate populations of interneurons. None of the GFP-ir interneurons are immunoreactive for CR. Most GFP-ir cells in the GL also express CB, while a few did not label with the CB antibody (pointed by arrows in B and C). PG cells that are positive for CB only are pointed by arrowheads. Scale: A, E and F, 20μm. B, C and D, 10μm.

Table 1

VAChT fiber density in bulbar layers (fibers/(100 μm)^3)

OB layer	Contr. OB	Ipsi. OB
GL	888 ± 51	216 ± 61
EPL	333 ± 51	26 ± 7
IPL	1054 ± 25	209 ± 37
GCL	613 ± 98	237 ± 84

Density ± SEM, n = 3 olfactory bulbs

Contr: contralateral. Ipsi: ipsilateral

Table 2

ChAT(GFP)-expressing interneurons in bulbar layers

	OB Layer			
ChAT-GFP Expressing Cells	**GL**	**EPL/MCL/IPL**	**GCL**	**Whole bulb**
Counted Cells [*] *Mean*	2490	529	76	3095
Range	1623 - 3724	375 - 735	14 - 156	2437 - 4387
Cell Density (cells / mm^3) [**]	20992 ± 2630	2249 ± 262	685 ± 160	
Estimated Cells in a bulb	30440 ± 3775	5557 ± 648	1110 ± 260	37106 ± 3706

n = 8 OBs from 8 mice.

[*] Count from random regions in images from 1/6 of whole OB sections.

[**] Mean ± *SEM*

Table 3

TH and CB immunoreactive cells and colocalization with ChAT(GFP)-expressing cells in bulbar layers

	OB Layer			
	GL	**EPL/MCL/IPL**	**GCL**	**Whole bulb**
TH+ cells *n = 3 OBs from 3 mice*				
Cell Density (Cells / mm^3)	29278 ± 380	573 ± 49	19.4 ± 5.2	
ChAT-GFP+ cells / TH+ cells	0.64 ± 0.06	3.83 ± 0.83	28.1 ± 12.1	0.76 ± 0.04
Colocarized with ChAT-GFP (cells / mm^3)	0	0	0	0
CB+ cells *n = OBs from 5 mice*				
Cell Density (Cells / mm^3)	37556 ± 2201	807 ± 144	202 ± 38	
ChAT-GFP+ cells / CB+ cells	0.59 ± 0.09	3.18 ± 0.62	4.31 ± 1.54	0.63 ± 0.03
% of CB+ cells expressing ChAT-GFP	52.7 ± 6.3	53.7 ± 6.0	19.1 ± 12	52.4 ± 6.2
% of ChAT-GFP+ cells expressing CB	91.7 ± 3.4	18.2 ± 5.3	3.6 ± 1.4	76.6 ± 2.0

Mean ± SEM